CanariCam

Astronomers User Manual

Version 1.3
23 April 2009

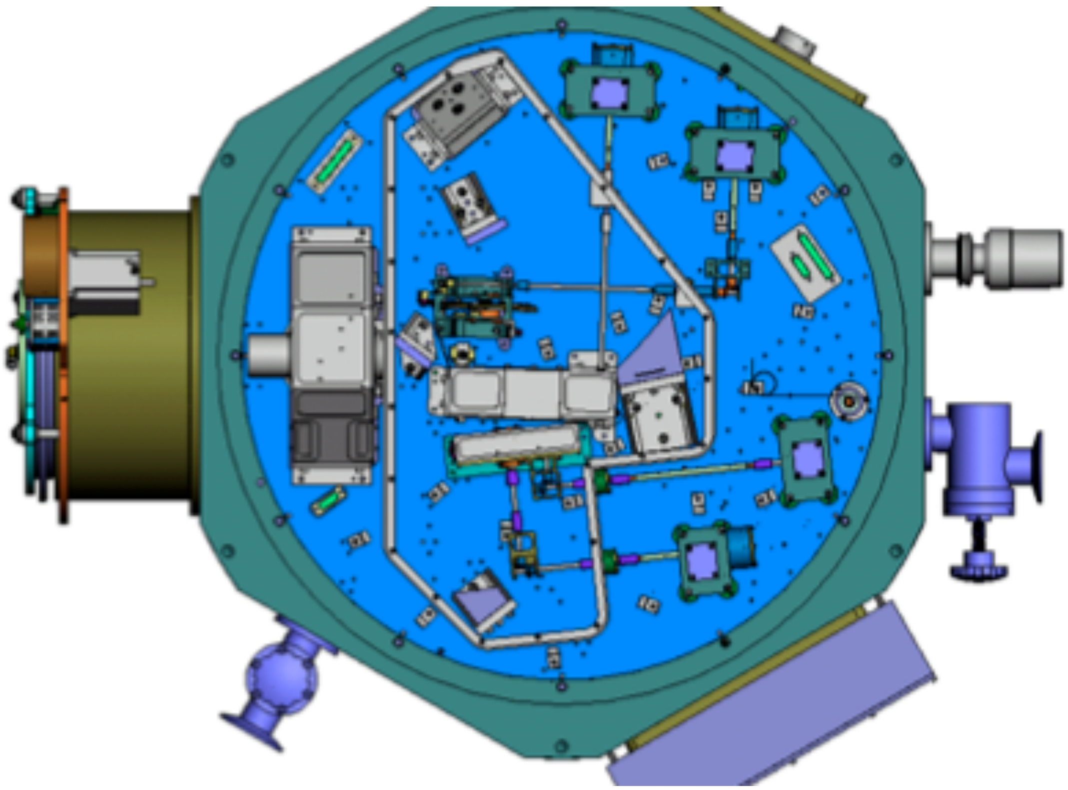

Prepared by Chris Packham and the CanariCam instrument team:
Charles Telesco, David Ciardi, Robert Piña, James Radomski, Francisco Reyes, Dan Cawlfield, Jim French, Kevin Hanna, Roger Julian, Jeff Julian, Margaret Moerchen, Frank Varosi

Preface

The purpose of this manual is to provide information regarding the use of CanariCam, the mid-IR multi-mode camera for the Gran Telescopio Canarias (GTC). CanariCam is a mid infrared (8-25 μm) imager, long-slit spectrograph, dual-beam polarimeter, and coronagraph built by the University of Florida Infrared Astrophysics Group for use at the GTC by the astronomical community. In this version of the document, certain assumptions are made regarding the system capabilities that are subject to change during commissioning. Specific questions about the system should be directed to the GTC Help Desk.

The CanariCam instrument team is heavily indebted to the T-ReCS instrument development team, as listed below, as well as the Gemini observatory, especially those persons listed below.

T-ReCS Instrument Development Team: Charles Telesco, Robert Piña, Chris Packham, David Ciardi, Francisco Reyes, Naibi Mariñas, James Radomski, Cynthia Gomez, Abdulatif Albusairi, Dan Cawlfield, Jim French, Kevin Hanna, David Hon, Roger Julian, Jeff Julian, Tom Kisko, Frank Varosi

Gemini: Tom Hayward, Kevin Volk, Rachel Mason, Scott Fisher, Jim DeBuizer, Kathleen Labrie, and many others.

Science Drivers

CanariCam will provide remarkable insight into the nature of a broad range of astronomical objects and environments. These advances will result from the powerful combination of the world's largest optical-IR telescope, the 10.4-meter state-of-the-art GTC, and the high throughput, excellent optics, and robust mechanical structure of CanariCam that will empower the astronomer with its versatile mid-IR coverage.

The design of CanariCam was driven by the broad range of scientific issues that it can address simply and elegantly. Objects at temperatures of ~100-1000 K emit significant mid-IR radiation. Of particular importance are the ubiquitous, small solid particles – dust – that absorb radiation at virtually any wavelength and re-radiate it as IR, sub-millimeter, or millimeter radiation. Mid-IR continuum emission from the dust is diagnostic of the properties of a large variety of astrophysical objects as diverse as star-forming regions, circumstellar disks, and starburst and active galaxies. With multi-wavelength mid-IR imaging, it is possible to locate the energy sources that power their often enormous luminosities, trace the distributions of the dust particles and their temperatures, and determine how UV and optical radiation, which heats the dust, propagates throughout the IR-emitting regions. Furthermore, the dust responsible for the often heavy visual extinction is significantly more transparent at mid-IR wavelengths, making mid-IR imaging an incisive and unique probe in complex, visually obscured environments. In order to be able to address the broadest range of astronomical problems, CanariCam obtains these images with negligible degradation to the image quality delivered by the GTC telescope.

Narrowband mid-IR imaging will be of tremendous value in determining key properties of the dust particles and in exploiting those properties to gain further insight into the nature of the IR sources. For example, mid-IR emission features at 7.7, 8.6, and 11.3 μm are attributed to polycyclic aromatic hydrocarbon molecules (PAHs), which are a significant constituent of the interstellar medium. The absorption of UV photons by a PAH molecule results in the emission of these features, the relative strengths indicating, among other properties, the molecular size. Particularly useful is the fact that these features are emitted by a PAH molecule *whenever* it absorbs the UV photon, independent of its distance from the UV-emitting source (e.g., a star). Since the PAHs are mixed in with the other dust (indeed, the PAHs are often considered to arise from very small dust grains), they should be traceable by their emission features at locations too distant from the heating source for the UV flux to heat a larger "classical" dust grain to a high enough temperature to emit significant mid-IR continuum radiation. Imaging with narrowband filters centered on the PAH and other features (e.g., the silicate features, the [NeII] 12.8 μm emission line, etc.) presents outstanding opportunities for exploration with CanariCam. The CanariCam spectroscopic mode will provide access to numerous emission and absorption features that will significantly enhance CanariCam's diagnostic power.

CanariCam incorporates for the first time a dual-beam MIR polarimeter for use at all wavelengths in the 10 μm window. This will provide a uniquely powerful diagnostic of objects as diverse as young stars, debris disk and AGN. Since all the polarimetry optics are cool and highly transmissive (>80%), polarimetry using CanariCam can be quickly implemented. In this manual, special attention is given to the data reduction of CanariCam polarimetry data in order to guide the non-polarimetry specialist. Finally, a coronographic mode is offered for all wavelengths in the 10 μm window. This mode will facilitate the investigation of faint objects near to relatively bright sources, such as brown dwarf candidates close to a bright 'parent' star.

Through broadband and narrowband imaging, long-slit spectroscopy, polarimetry and corongraphy, CanariCam will support the exploration of a uniquely informative spectral region at a telescope that is well placed for this exploration. Of the broad range of scientific programs that will be carried out at the GTC, those in the mid-IR will likely gain the most from GTC's low emissivity and the outstanding Observatorio del Roque de los Muchachos (ORM) site characteristics. This advantage is dramatically apparent when one realizes that, in the background-limited regime that applies to the mid-IR region, the integration time required to achieve a given signal-to-noise ratio for a point source scales inversely as the telescope aperture diameter *to the fourth power!* Thus, remarkably, an observation takes 50 times less integration on the GTC than at a 4-meter class telescope, even if the difference in emissivity is ignored. These gains imply that previously impossible scientific programs can become routine with the GTC. The CanariCam design is driven by the science that takes full advantage of these opportunities.

TABLE OF CONTENTS

1 Instrument – Introduction

This manual is presented in four main sections: Section 1 gives an overview of the instrument, Section 2 describes the detector, Section 3 summarizes the optical information most relevant for users who are astronomers, and Section 4 provides useful general information about mid-IR astronomy, with the attached appendices containing additional information specific to the operation and configuration of CanariCam. In this version of the document, certain assumptions are made regarding the system capabilities that are subject to change during commissioning. Specific questions about the system should be directed to the GTC Help Desk.

1.1 The Camera

CanariCam is optimized for excellent image quality across the 8-26 μm window. The optical design is such that CanariCam is diffraction limited at 8 μm (Nyquist sampling the 8 μm PSF). The array is a 320x240 Si:As blocked impurity band (BIB) device with a pixel scale of 0.08"/pixel providing a total field of view of 28.4"x 21.1". There are three powered mirrors and five folding flats (four fixed and one movable on the grating turret). All the mirrors are gold coated, which provides a combined reflectivity of ~92%.

CanariCam is equipped with a suite of narrow-band and broad-band 10 and 20 μm filters, located within two filter wheels immediately after the Lyot-stop wheel at the first pupil image. To reduce the cryogenic instrument size, the optical layout is folded, with the optics located on two sides of the optical bench. The two sides are connected optically only through a pair of folding flats (F3 and F4), with the bench itself serving as a very affective baffle reducing stray light that can reach the focal plane.

In addition to the normal field-imaging mode, CanariCam is capable of both pupil and window imaging. Pupil imaging is achieved by re-imaging the first pupil image onto the focal plane with a ZnSe relay lens. The pupil-imaging mode is used to ensure that CanariCam is optimally aligned with the telescope optical axis. This diagnostic capability is particularly important, since CanariCam can be mounted at any one of several different focal stations (Nasmyth, the up-looking (straight cassegrain) port, or the side-looking (folded cassegrain) port), each of which will have slightly different alignment constraints.

The window–imaging mode permits one to monitor the health and status of the dewar windows. Several windows are mounted on a plate attached to the dewar with a ferrofluidic feedthrough, so that any one of the windows can be inserted into the beam during normal operation. This window-changer assembly thus permits one to optimize the window material for specific ambient observing conditions and scientific observing requirements. Window imaging allows the observatory to maintain a record of the quality of each of the windows to determine if a particular window may need replacing.

1.2 The Spectrograph

CanariCam is designed to be a low-to-moderate-resolution spectrograph at 10 and 20 μm. Four gold-coated plane diffraction gratings are located on a rotating grating turret. In spectroscopic mode, the gratings replace the folding flat located on the turret. The two low-resolution gratings cover the entire 10 μm window (R≈175; $\Delta\lambda$ = 7.5–13.5 μm) and the entire 20 μm window (R≈120; $\Delta\lambda$ = 16.0–25.0 μm). The 10 μm moderate-resolution grating (R≈1300) spans $\Delta\lambda \approx 0.65$ μm (when centered at 10.5 μm) and requires several settings (dependant on the amount of wavelength overlapping required) to cover the entire 10 μm atmospheric window. The 20 μm moderate-resolution grating (R≈890) spans $\Delta\lambda \approx 0.45$ μm (when centered at 20.5 μm) and also requires several settings (dependant on the amount of wavelength overlapping required) to cover the entire 10 μm atmospheric window. The spectrum is dispersed along the long axis of the array (320 pixels). For each of the low-resolution grating settings, the spectral-resolution element is sampled by approximately five pixels. The slit lengths are oversized to ensure that the slits span the entire short dimension of the array.

Nine slits are available, offering flexibility in matching the wavelength of operation or the seeing conditions.

1.3 The Polarimeter

CanariCam uses a CdSe Wollaston prism and half wave retarder (half wave plate, HWP) to provide dual beam polarimetry at all wavelengths in the N band window. The peak accuracy of the instrument >99% at 10.5μm, but rolls off significantly toward the cut-on/off of the N band window. Correction for this will investigated as part of the commissioning process on the GTC and described at a later date. To eliminate overlapping of the orthogonally polarized beams on the array, a focal plane mask is used in the aperture wheel.

All parameters for CanariCam polarimetry are the same as those for imaging, but around 50% of the field of view is blocked by the focal plane mask. Also, observing efficiency is slightly lower due to the repetitive motion of the HWP. Nevertheless, CanariCam polarimetry represents the first dual-beam MIR polarimeter and hence opens the door to a near era of high precision MIR polarimetry.

1.4 The Coronagraph

CanariCam has the first mid-IR coronagraphic mode ever used at a major ground-based observatory. This mode improves the ability to detect faint mid-IR point sources, such as sub-stellar objects, and faint extended sources, such as circumstellar disks, that are located very close to bright point sources and which might not be detectable without the coronagraphic mode.

To implement this mode, one inserts an occulting-spot mask at the telescope focal plane and a pupil mask at the first pupil plane inside the camera. In the initial implementation of this mode, the occulting spot is a sharp-edged ("top hat"), opaque metal disk with a radius of 0.84 arcsec, which corresponds to $\lambda/5$ at 8 μm and $\lambda/4$ at 10 μm. This mask is painted black and is attached to the center of a thin ZnSe disk that is inserted into the focal-plane mask-wheel. The pupil mask consists of a small central opaque disk, which blocks the central obscuration in the pupil image, and a large hexagonally shaped mask that blocks the outer edges of the primary mirror. The central opaque disk of the mask is 140% the size of the image it is masking, and the outer hexagonal mask is 90% the size of the edge of the pupil image it is masking. The disk-shaped central part of the pupil mask is supported by thin, slightly wedged, veins that mask the images of the secondary-mirror spider supports. With the occulting and pupil masks in place, the total throughput of the coronagraphic mode is about 66% that of the regular imaging mode.

At the beginning of an observing sequence, one must have the bright star centered on the occulting spot and the pupil mask rotated so that the spiders are masked (see below). The pupil mask is mounted in a holder that rotates in coordination with the rotation of the pupil, which occurs as the alt-az telescope tracks an astronomical source across the sky. However, the motor that rotates the mask cannot be turned on during data acquisition (which would introduce noise), so pupil-mask rotation can only be permitted while the telescope is beam-switching ("nodding") to its alternative position. It is for this reason that the spider mask is somewhat oversized (20 times the actual image) and slightly wedge-shaped.

At the time of this writing, the final procedure for centering a star on the occulting spot has not been fully determined. The final procedure will depend on detailed telescope performance and will be revised during on-sky commissioning of CanariCam on the GTC. However, the following procedure is one likely scenario for setup. During normal operation of the coronagraphic mode with both masks inserted into the beam, one centers the stellar image behind the occulting spot by moving the telescope first in right ascension, centering in time, then in declination, also centering in time. By "centering in time" we mean measuring the time, at very slow slew, to move the stellar image from one side to the other side of the occulting mask (i.e., from disappearance behind the mask to reappearance). Final adjustment of the stellar location is made by switching to the pupil-imaging mode and making fine motions of the telescope that minimize the stellar flux in quick-look frames. While still in the pupil-imaging mode, the pupil mask is then rotated until the observer sees that the spider veins (which emit mid-IR radiation) are blocked by the veins of the mask. The spider mask should initially be positioned so that the spider image is blocked by, but at one side of, the mask. During data acquisition, the mask will not move, but the pupil image will rotate; during the telescope beam-switch ("nod"), the motor is turned on and the pupil mask is rotated to compensate for the pupil-image rotation that occurred during the previous data acquisition.

Obviously, with the occulting mask in place, any faint point or extended source around a bright object such as a star must be farther away than 0.84 arcsec from the star to be detected. Simulations indicate that under good sky conditions, the PSF suppression ratio (the ratio of the residual point-spread-function (PSF) to the un-occulted PSF) can be as good as 10%. Since much or all of the noise associated with detecting a faint source near a bright source is due to PSF subtraction, the ability to use coronagraphy to decrease the PSF wings by a factor of ten can reduce that "subtraction" noise so low that the observations can become background limited. Once the above procedures associated with implementation of the masks is followed, then the observations proceed as normal imaging observations.

1.5 Basic Instrument Characteristics

Detector Pixel Format:	320 x 240
Science Operating Wavelength Range:	7.5-26 μm
Pixel Scale:	0.08 arcsec $pixel^{-1}$
Field of View:	25.6 x 19.2 arcsec
10 μm Low-Resolution Spectroscopy:	$R=\lambda/\Delta\lambda=175$ near 10.5 μm
10 μm High-Resolution Spectroscopy:	$R=\lambda/\Delta\lambda=1300$ near 10.5 μm
20 μm Low-Resolution Spectroscopy:	$R=\lambda/\Delta\lambda=175$ near 20.5 μm
20 μm High-Resolution Spectroscopy:	$R=\lambda/\Delta\lambda=890$ near 20.5 μm
Coronagraphic Mode:	Any λ within the N band
Polarimetry Mode:	Dual-beam at any λ within the N band

CanariCam uses a Raytheon CRC-774 320 x 240 Si:As, blocked impurity band (BIB), or impurity band conduction (IBC), high-background infrared Focal Plane Array (FPA). The detector has excellent cosmetic quality. Figure 1 shows an image of the detector under uniform illumination in standard chop mode. There are no dead pixels. Some of the key detector characteristics are:

Detector:	Raytheon CRC-774 320 x 240 Si:As IBC
Physical Pixel Size:	50 x 50 μm
Full-well Capacity:	1.0e7 or 3.0e7 electrons (high or low gain)
Array Readnoise:	Deep well: 3.6 ADU or 2060 e^-
	Shallow well: 4.6 ADU or 828 e^-
Dark Current:	≤ 100 electrons/sec @ T = 6 K
Quantum Yield:	>40% at peak
Number of Output Channels:	16

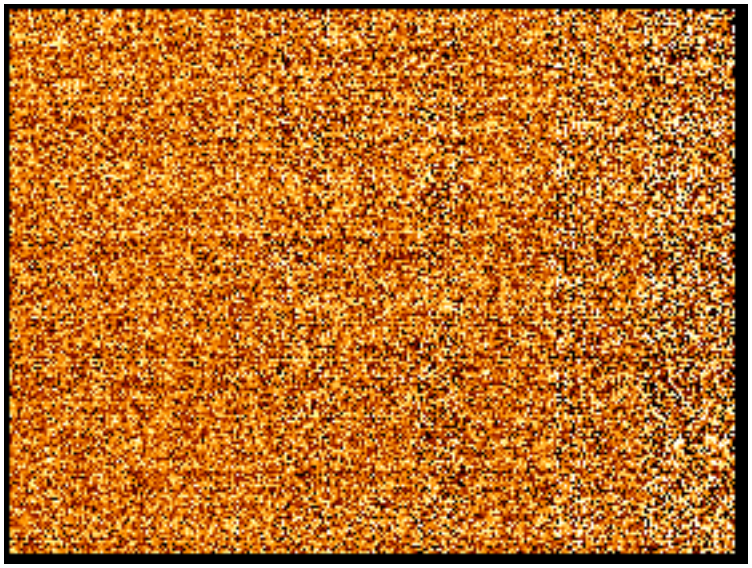

Figure 1. Dark (cold internal blankoff) chopped image (see Appendix A, Section II.I) taken with CanariCam.

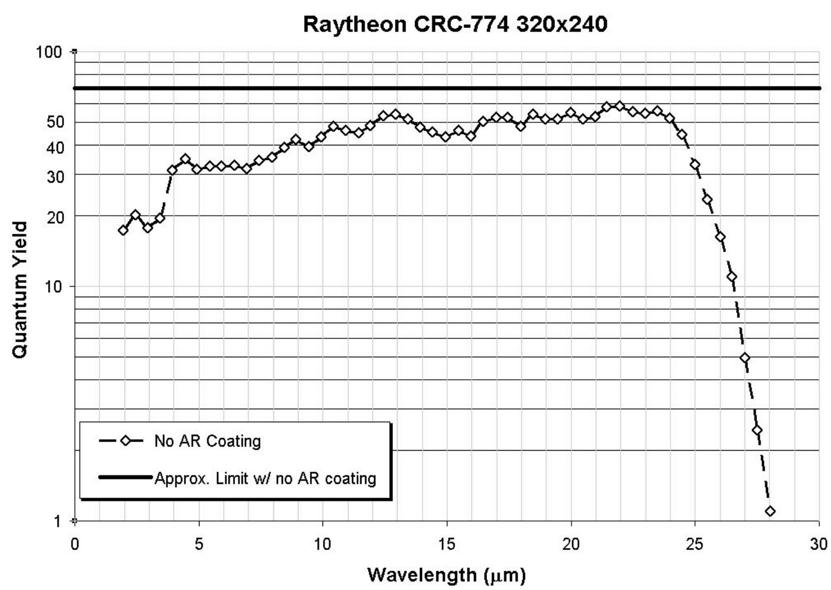

Figure 2. Quantum yield (percent) of a typical Raytheon CRC-774 320 x 240 Si:As IBC detector.

1.6 Detector Readout

Several mid-IR instruments on large telescopes use the Raytheon CRC-774 320 x 240 Si:As IBC detector array. These include COMICS on the Subaru 8-m (Kataza et al. 2000), Michelle on the Gemini North 8-m (Glasse et al. 1997), the new decommissioned TIMMI-2 on the ESO 3.6-m (Reimann et al. 1998), and of course T-ReCS on the Gemini South 8-m (Telesco et al. 1998). We note that the VLT's VISIR mid-IR instrument currently uses a 256x256 Boeing array. To date, the Raytheon device remains the largest format mid-IR array in astronomical use. However, this device displays several unwanted effects when exposed to a very bright source. Below we discuss these effects as well as readout methods used to reduce them. It may be helpful in considering these effects to keep in mind that each contiguous group of 20 vertical columns is read out through one of the 16 output channels (i.e., columns 1-20 are readout through channel 1, columns 21-40 are readout through channel 2, etc.). In addition, the first pixel read out in each channel is the lower-left one as displayed in Figure 1, and the last is the upper right one.

1.6.1 Single-Point Sampling (S1)

Artifacts associated with the imaging of a bright source are most noticeable in the S1 sampling mode. These effects, sometimes referred to as a level drop or "drooping," have been well documented by the COMICS team[1] (Okamoto, Y. K. et al. SPIE 2002; Sako. S., et al. PASP, 2003). For convenience, we follow the labeling convention set out in those papers. The artifacts can be classified into four types:

- **Pattern 1** – a gradation in brightness spanning, and restricted to, a single channel and diminishing in brightness on the downstream pixels (in terms of readout direction, which is "up" on the displayed image).
- **Pattern 2** – a negative offset in the same *"column"* as the peak of a bright source.
- **Pattern 3** – a negative offset in the same *"row"* as the peak of a bright source.
- **Pattern 4** – a horizontal (see displayed image) sequence of negative spots along the entire row where the bright source is positioned.

Figure 3, which is courtesy of the COMICS team, shows all four effects.

The negative-offset, or level-drop, Patterns 1 and 2 are due to the transient variations of the characteristics of the source-follower circuits used to read out the array when the input signals are drastically changed, as occurs during read-out of a bright source. The negative-offset, or level–drop, Patterns 3 and 4 are due to the variations of the bias voltages when the input signals are changed due to a bright source.

[1] The CanariCam teams expresses its deep thanks to the COMICS team who have kindly provided numerous materials about the Raytheon array and their improved read-out technique – domo arigato gozaimasu.

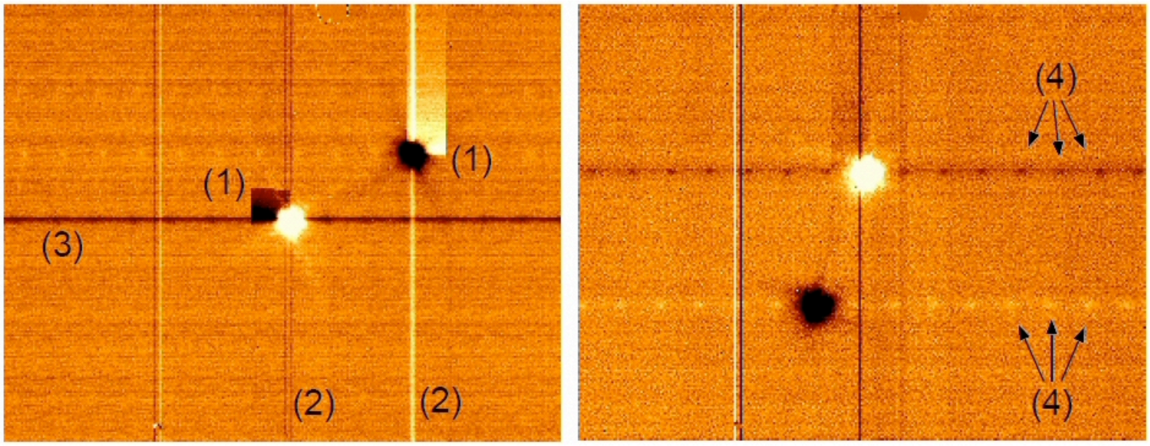

Figure 3. Image of bright star taken with the instrument COMICS on Subaru. Four negative offset, or level-drop, effects are shown in these images as described in the text

1.6.2 Correlated Quadruple Sampling (S1R3)

Effects 1 and 2 can be eliminated by using a readout method called Correlated Quadruple Sampling (CQS), which consists of referencing the detector ramp voltage to several of the silicon multiplexor (or "mux") internal voltages. In order to reduce Patterns 3 and 4 which are seen only when observing very bright objects, analytical corrections are required in addition to CQS. These analytical corrections are not generally available, as the effects are a function of the frametime, source brightness, and other variables. Though noticeable, this effect is relatively small in CanariCam, resulting in only a 0.1% - 0.6% effect in signal, as determined from the ratio of the source peak signal to that of the negative offset. The exact level of that offset is dependant on the frame time and source intensity, but not the distance from the source (see below for a detailed discussion based on our laboratory tests). It appears that this artifact may be partially eliminated by referring to channels that show the spots but contain no source.

Although these methods effectively eliminate or greatly reduce readout artifacts associated with the Raytheon CRC-774 detector array, they also introduce new operating limitations, as follows:

- Since CQS requires four times the data to correct for patterns 1 and 2, the frametimes must be approximately four times longer. Thus the minimum frametime for CanariCam of ~5 ms is effectively increased to ~20 ms. While not limiting most observations with CanariCam, it does hamper observations using broad-band filters such as N-band and Qw-20.8μm. These wide pass-band filters expose the detector to high thermal backgrounds from the sky and telescope. Thus, the array must be read out quickly, typically at <20 ms, so that broad-band observations may be difficult or impossible with CQS.
- Another effect of CQS is to increase the readout noise, because the net signal is derived from four times the data. However, this has no significant effect on imaging

or low-res spectroscopy where noise is dominated by the background. It may, however, reduce sensitivity in the high-resolution spectroscopy modes.

- Finally in order to correct for artifacts 3 and 4 one must have at least one channel not overlapping the astronomical source in order to provide a reference that can be subtracted. This may be difficult in the case of extended bright sources and spectroscopic data of bright sources. Further characterization of this phenomenon will be made during on-sky commissioning of CanariCam on the GTC, and one should check the CanariCam WWW page for the latest information.

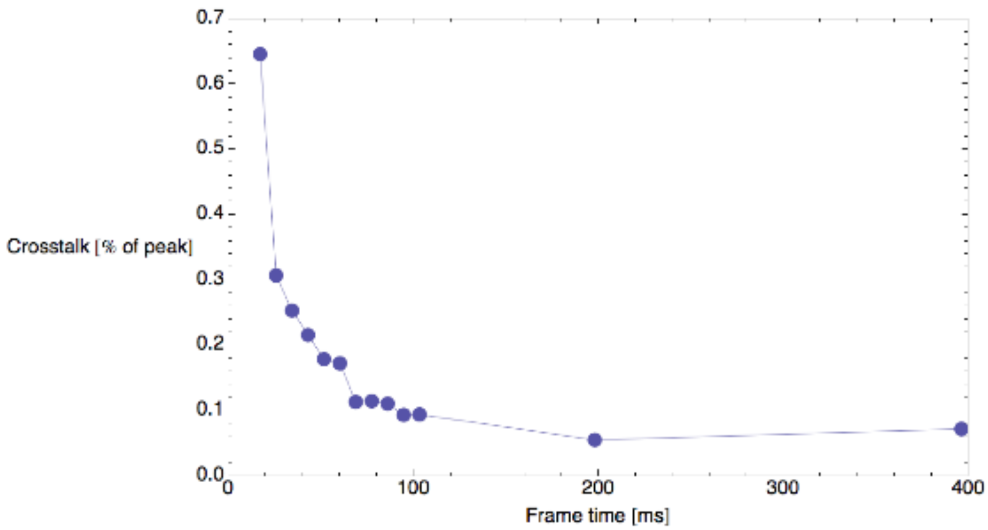

Figure 4. Percentage of level drop vs. frame time. Level drop percentage is calculated by taking ratio of source peak to level-drop minimum.

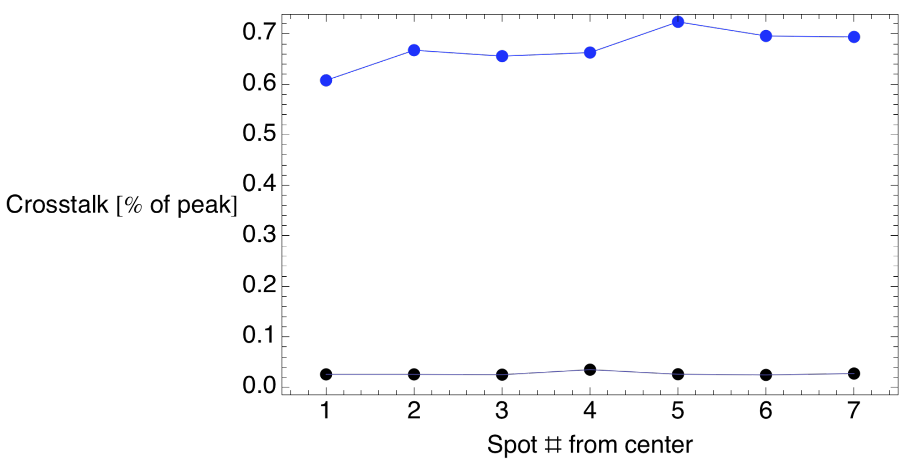

Figure 5. Percentage level drop vs. spot number from center as measured in two different filters and thus two different flux levels. Level drop percentage calculated by taking ratio of source peak to level-drop minimum.

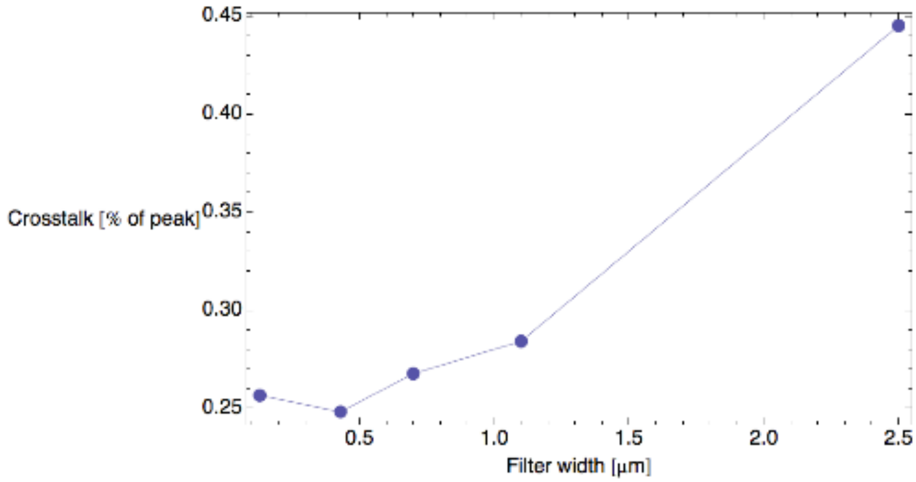

Figure 6. Percentage of level drop vs. flux level, as changed in the laboratory by increasing the filter bandwidth. Level drop percentage is calculated based on taking the ratio of the source peak to that of the level drop minimum.

To conclude the discussion on cross-talk of the CanariCam array, we stress that it is only a noticeable effect for very bright objects. While it may appear prominent, the amount of 'negative-flux' is quite small, and therefore affects on photometry are usually insignificant. For observing faint sources near a bright object, however, one may want to consider use of the coronographic mode, which will eliminate any cross-talk problems.

1.7 Mid-Infrared Flat Fielding

Flat-field frames are needed to permit correction for fixed-pattern noise in the array. There is no standard method for obtaining accurate flat fields in the mid-IR. Inaccurate flat fields can leave residual fixed-pattern noise, or worse, actually add noise and structure to the science data. Currently flat fielding techniques are still in the development and test phase for CanariCam. Other discussions of techniques used for mid-IR flat fielding can be found for the mid-IR instrument TIMMI2 (Reimann et al. 1998; see online manual). Below is a short discussion of flat fielding in the mid-IR as it applies to CanariCam.

In the optical, flat fields are typically taken at the end of the night by observing either a screen mounted on the dome or the sky to provide uniform illumination on the detector. However, in the mid-IR, dome flats are unusable, because the screen, which is a room temperature blackbody, will generally saturate a mid-IR detector through most passbands. In order to create a mid-IR flat field at least two images with levels of background illumination different from each other by a few percent are needed. Subtracting the lower–background image from the higher-background image provides a map of the spatial variations in sensitivity of the pixels across the array. One method by which this can be achieved is to observe the sky at low airmass and at a higher airmass. The background level increases with increasing zenith distance and atmospheric optical depth, which results in the images being taken at both a low and a high background. Another method permits taking the flat field near in time and location to the science observation. This is done for CanariCam by use of the Sector Wheel (Section 2.2), which contains a polystyrene mask. This mask can be rotated into the beam to increase the thermal background and provide a high-background image. However, this methodology is still in an experimental phase. We note that in the case of T-ReCS on Gemini South flat fields are rarely used, due both to the difficulty in their production and that they may actually introduce more noise than they remove. Hence, at this time we do not recommend that flat fields are taken for CanariCam data.

1.8 Detector Temperature Control

The power dissipation of an IBC/BIB array depends strongly on the background photon flux illuminating the array. For example, the power dissipation of the Boeing 128×128 Si:As BIB high-flux device (HF-16; used in the University of Florida mid-IR imager/spectrometer OSCIR) increases by a factor of two when going from zero-flux (i.e. blanked off) to high-flux illumination (e.g. broadband N imaging). Without temperature control, this increase in power dissipation results in the array temperature increasing by ~0.6 K and a change in detector responsivity of ~30%. This variation of detector response makes the repeatability of calibration measurements and flat-fielding potentially problematic if the detector is not maintained at a stable temperature. The required detector temperature stability is on the order of a few 0.01 K.

In the laboratory, the temperature at which the detector sensitivity is maximized was determined to be 9 K. This will be the target value for the detector temperature control. During normal operations, filter changes and telescope slews can produce large thermal flux variations on the array and correspondingly large variations of detector power dissipation. Due to the finite response of the closed-loop temperature control system, it may typically take a few seconds for the detector temperature to settle to the control temperature to within the stability requirement. *No observation should begin until the temperature reaches the required level. The CanariCam Instrument Sequencer will be designed to enforce this unless manually overridden.*

2 Instrument – Optics

Here we describe the function and key properties of each component in the optical train, beginning at the entrance window and proceeding along the light path to the detector. All mirrors are gold-coated, diamond-turned aluminum, and all internal wheels are moved with cold stepper motors. Many mechanisms such as the Aperture, Pupil, and Lyot Wheels contain components that will usually be inserted by GTC staff at the beginning of an observing run and remain unchanged during the run. Figure 7 shows the optical design for CanariCam.

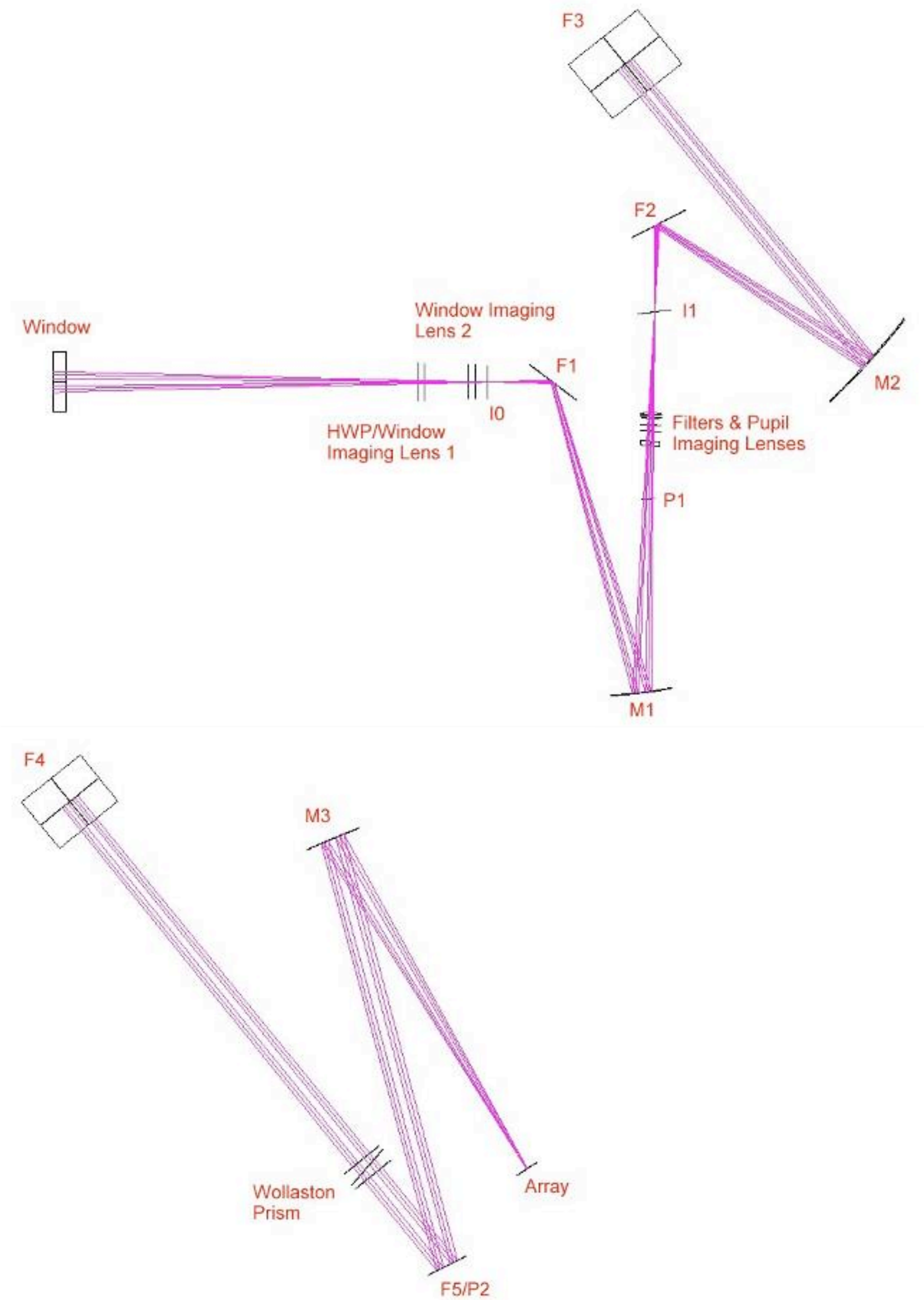

Figure 7. Sketch of the optical layout of CanariCam. The optical train on the upper deck of the optical bench is at left and the optical train on the lower deck is at right. Optics after the F3 folding mirror are located on the lower deck of the optical bench.

2.1 Dewar Entrance Window

Maintaining a high-quality entrance window is essential for CanariCam to routinely achieve its performance requirements. Windows must be clean, dry, and largely free of scratches to reduce scattering of light and to avoid significantly increasing the thermal emission that would reduce frame times and increase the background ‘photon-noise’. Furthermore, since CanariCam must remain at low temperature and on the telescope for months at a time, the entrance window assembly must be robust enough to ensure that the windows are well protected from dust and moisture for long periods of time and under sometimes-harsh conditions. Degradation of windows by water is a particular concern, since some of the window materials are water-soluble. To address these issues and concerns, CanariCam employs a window-turret design in which the cryostat window changer is used to select the optimum window for the selected instrument configuration, wavelength of observation and environmental conditions (in particular, humidity). It utilizes one stepper motor and has the following five positions: ZnSe window, KBr window (in two of the positions), KRS-5 window, and two blanks (one is mirrored and gold coated to minimize background radiation during long periods when CanariCam is not in active use). Only the “active” window is physically exposed, all the others being protected by a housing that is continuously purged by (dry) N_2 gas. The active window is also bathed in dry gas. In the protected position an aluminum blank is used in place of a transmissive window, so that none of the windows is exposed when the instrument is not in operation. An external, warm stepper motor rotates the wheel so that any of the windows can be rotated into the incident beam. Table 1 summarizes the properties of the window materials. Figures 6-8 shows the transmission curves for each window as provided by the window vendor Janos Technology. Also in each figure, in the bottom panels, are shown measured (but with limited wavelength coverage) transmission curves for CanariCam (where there is overlap in the graphs, the measured graphs should be adopted).

Table 1 Entrance Window Parameters

Window	Diameter	Thickness	Coating	Emissivity
KRS-5	48 mm	6.0 mm	none	0.3%
ZnSe	50 mm	6.0 mm	BBAR	0.4%
KBr-coated	50 mm	10.0 mm	Humidity Protectant	?
Block	Safe Storage Position			
Block-mirror	Mirrored safe storage position			

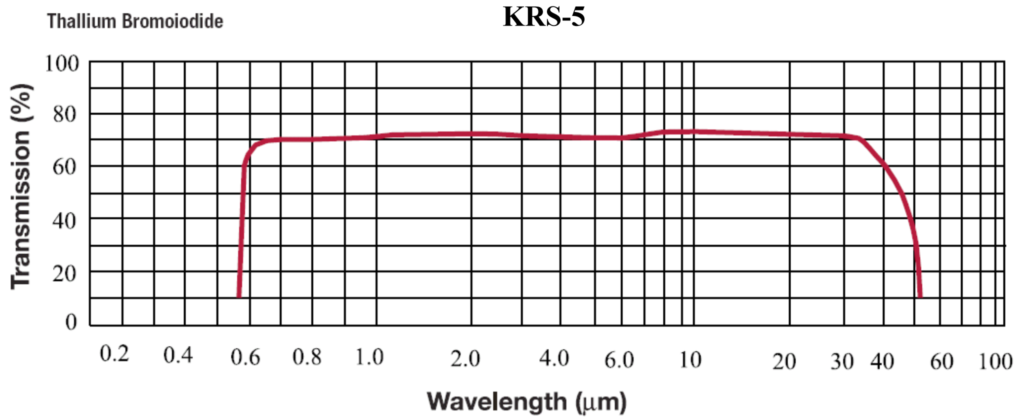

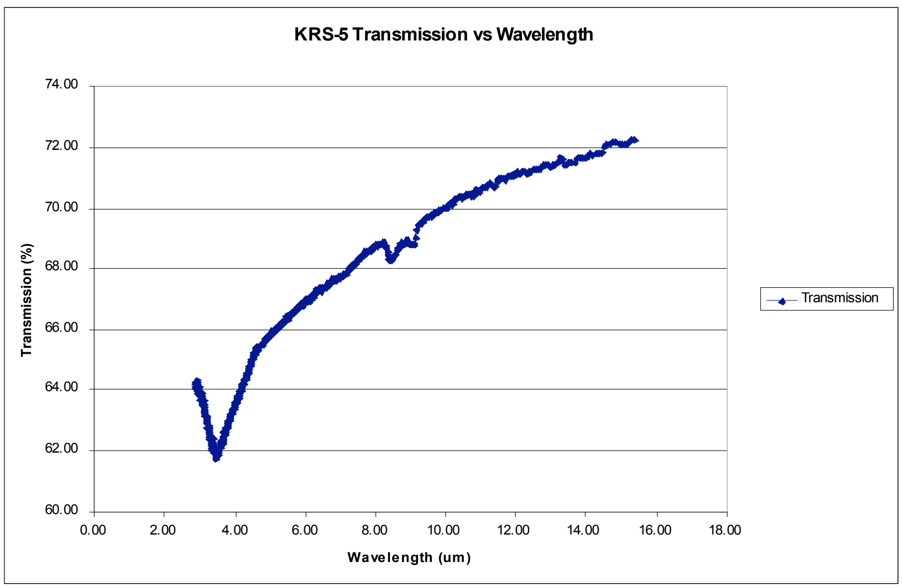

Figure 8. Transmission curve for KRS-5 window: estimated (top), measured (bottom).

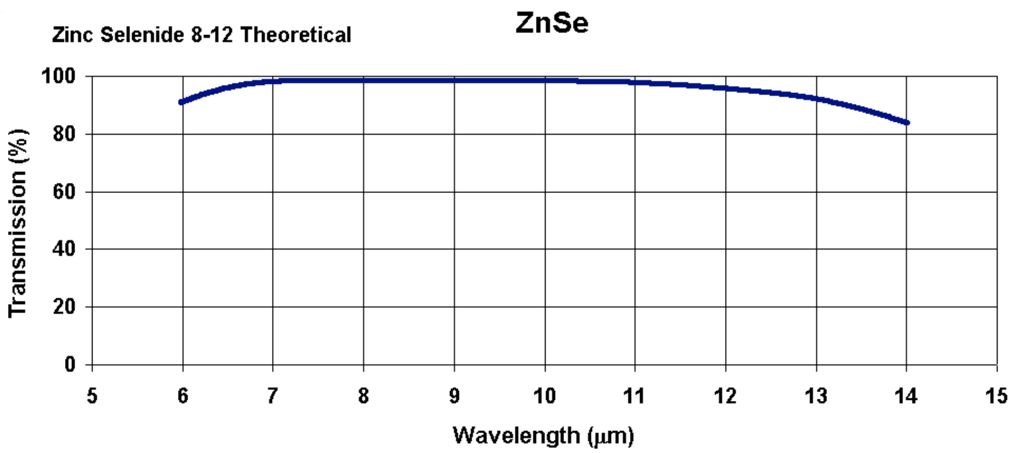

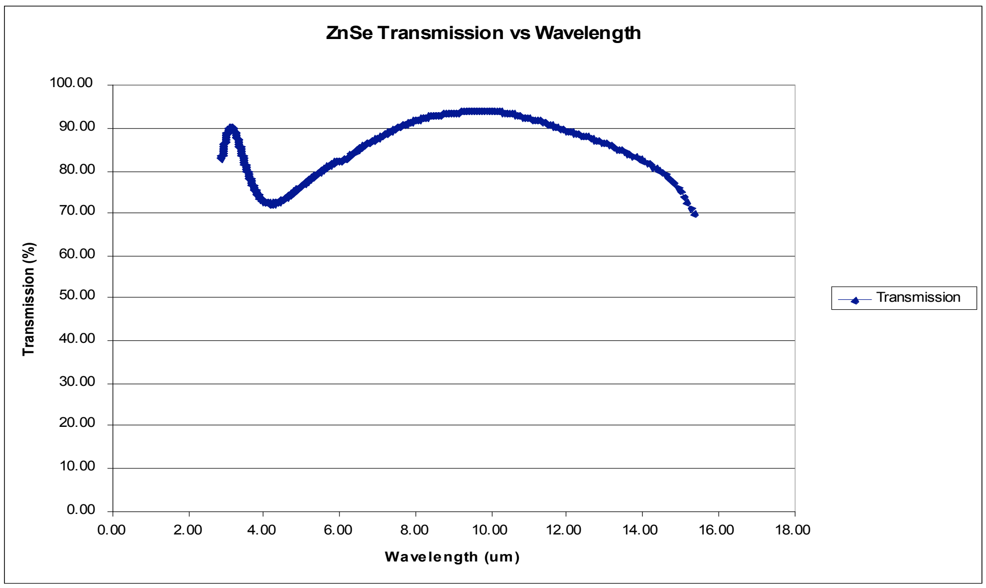

Figure 9. Transmission curve for ZnSe window: estimated (top), measured (bottom).

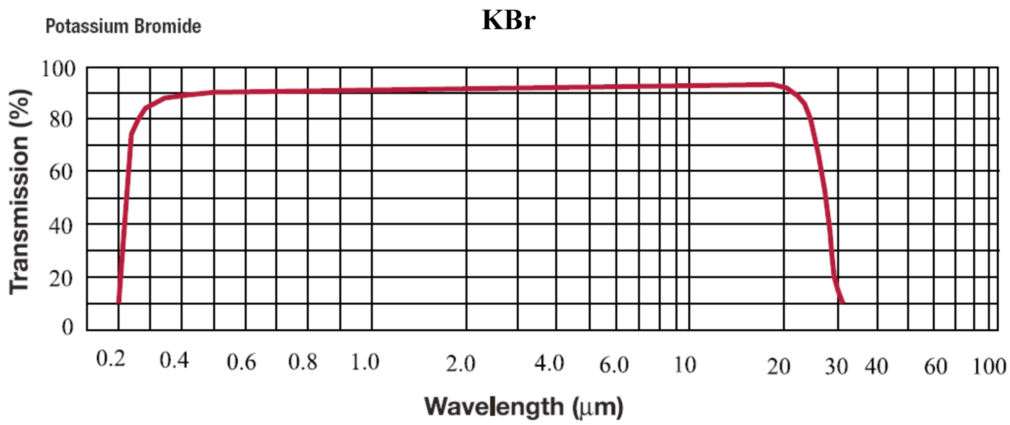

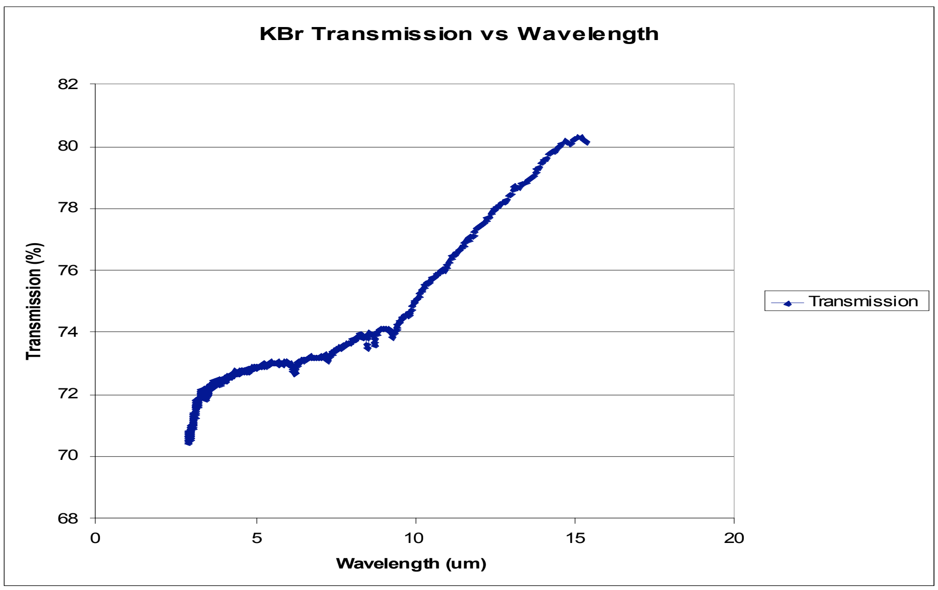

Figure 10. Transmission curve for the KBr window: estimated (top), measured (bottom).

2.2 Sector Wheel

Outsider the dewar and just in front of dewar window is the sector wheel (not shown in Figure 7). The sector wheel contains four positions, one of which is open (clear). The other three positions contain spectrally flat sources that are currently being tested for use in creating flat fields for both imaging and spectroscopic modes. Also in this wheel is the wire grid polarizer, used for calibration of the polarimetric modes of cc.

Table 2 Sector Wheel Positions

Sector Wheel Position	Comments
Open	Open hole (normal operation)

Wire Grid	Polarizer for polarimetric calibration
Black Plate	High blackbody (for flat fielding)
Polystyrene	Increases background (for flat fielding)

2.3 Half Wave Plate Wheel

To minimize any instrumental polarization, the half-wave plate (HWP, sometimes called the half-wave retarder) wheel is the first optical component after passage through the entrance window. This wheel can accommodate up to three HWPs, but currently only the 10 µm HWP is installed. In the future, a second HWP may be purchased and installed, possibly to cover the 20 µm waveband or to provide achromatic polarimetric retardation versus wavelength. The HWPs can be rotated to four position angles (0°, 22.5°, 45° and 67.5°). The retardance/efficiency versus wavelength, and the laboratory transmission of the combined HWP and Wollaston was measured to be 83% at 10.5µm.

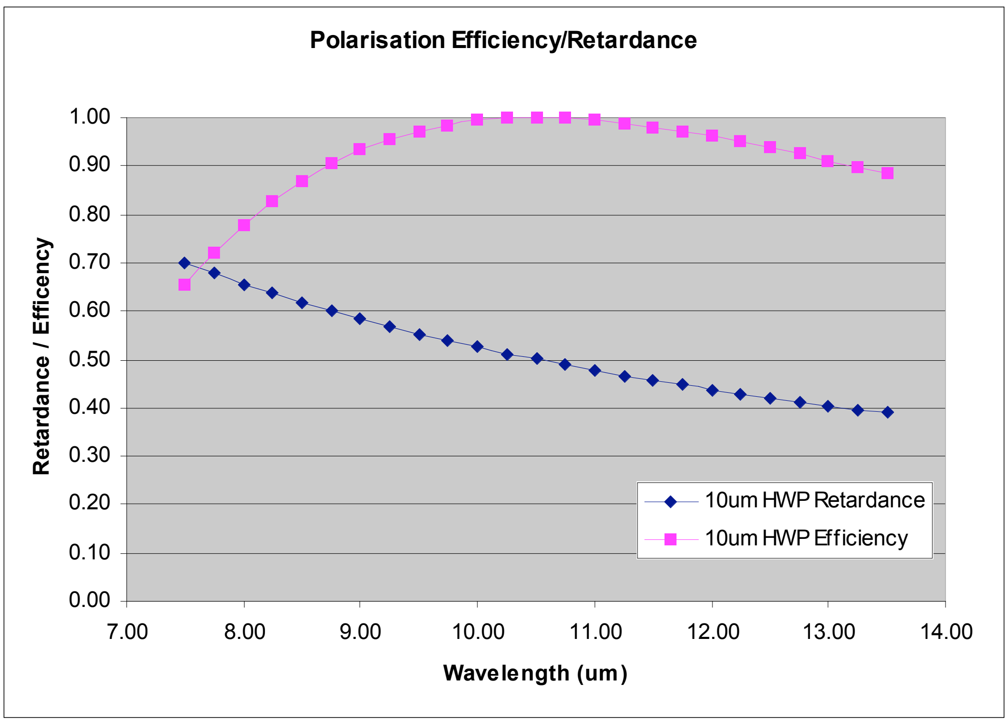

Also located in the HWP wheel are the window-imaging lenses, which allow inspection of the window quality to confirm optimal throughput and minimize background. The window-imaging mode is an engineering mode and is not expected to be used by astronomers. The full wheel is listed below.

Table 3 HWP Wheel Positions

HWP Wheel	Description
Open	Open for standard observations
HWP 10µm	HWP for 10µm polarimetric observations

Window Imaging	Window imaging lenses
Open (HWP1)	First spare position for a future HWP
Open	Open for standard observations
Open (HWP2)	Second spare position for a future HWP

2.4 Aperture Wheel

The aperture wheel is located at the telescope focal plane and coincides with the entrance to the optics-train housing. This wheel contains a selection of two field stops, a mask containing 3 pin holes, a pinhole grid, two polarimetric field masks, two coronagraphic masks, a slit dekker (not needed), and a blank disc. Aperture positions are summarized below in Table 4.

Table 4 Aperture Wheel Positions

Aperture	Description
Field Mask 1	10% oversized field mask (default mask)
Field Mask 2	20% oversized field mask
Polarimetric mask 1	Polarimetric mask for imaging- and/or spectro-polarimetric observations
Polarimetric mask 2	Polarimetric mask for imaging- and/or spectro-polarimetric observations. Unused in current CanariCam configuration.
Coronagraphic spot alpha	Coronagraphic spot – to be characterized during commissioning
Coronagraphic spot alpha	Coronagraphic spot – to be characterized during commissioning
Alignment spots	3 pinhole spots (400, 100 and 400μm diameter) used for alignment and image quality check-out
Alignment grid	Grid of pinhole spots (100μm diameter) used for alignment and image quality check-out
Slit dekker	Can be used in spectroscopic mode to reduce background light – unlikely to be needed during standard observations, to be confirmed during commissioning
Blank	Blank to stop light passing past the aperture wheel

2.5 Lyot Wheel

The Lyot stop is a crucial thermal baffle in the CanariCam optical system. The Lyot wheel contains 4 positions at which are located the masks listed in Table 5. The Lyot wheel contains pupil masks for optimal thorough-put and/or rejection of scattered and/or diffracted light. Generally, observers do not need to configure the Lyot wheel, since it is configured automatically by the observing system or the support astronomer.

Table 5 Lyot Wheel Positions

Lyot position	Description
Circular Mask 1	Inscribed to maximum filled pupil
Rose Petal Lyot	Lyot mask, most likely used only in the coronographic mode. The 6 segments (as defined by the GTC's spider) are reminiscent of a rose petal
Circular Mask 2	Circumscribed to maximum (partially-filled) pupil
Circ+8	Circular aperture for science use (8% larger than projected pupil size)

2.6 Filter Wheels

CanariCam has two filter wheels located just downstream from the Lyot wheel. There are 13 positions in each filter wheel for a total of 26 available positions. Currently six positions are either open or used for engineering tasks (including the pupil imaging lenses used to optimize pupil alignment of the instrument to the GTC). The other 20 positions contain 1-inch-diameter circular filters for astronomical use. Table 6 presents a summary of the filter characteristics[2]. The filter curves are shown in the GTC's CanariCam WWW page. In addition, there is a very slight, but noticeable, difference among some of the filters in the optical beam direction after passage through the filters. This results in a slight shift in the location of an astronomical image as one changes filters.

Table 6 Summary of Filters

Filter Name	Central λ [μm]	Bandwidth [μm]	Peak Trans. (%)	Temp. (K)	Comments
K	2.20	0.39	~78%	77	For Engineering Purposes
L	3.77	0.68	~93%	77	For Engineering Purposes
M	4.70	0.55	~92%	77	For Engineering Purposes

[2] Further information on the specific filter characteristics is available from the CanariCam WWW page or in the CanariCam Optical Design Manual.

Filter Name	Central λ [μm]	Bandwidth [μm]	Peak Trans. (%)	Temp. (K)	Comments
N	10.36	5.2	94.6	15	[V], [G], Spectroscopic Blocker
Si-1	7.8	1.1	85.9	297	[G]
PAH-1	8.6	0.43	78.9	15	[V], [G]
Si-2	8.7	1.1	88.0	30	[G]
Ar-III	8.99	0.13	74.1	15	[V], [G]
Si-3	9.8	1.0	91.7	30	[G]
Si-IV	10.52	0.16	73.2	15	[V], [G]
Si-4	10.3	0.9	91.6	30	[G]
PAH2	11.3	0.6	76.2	15	[V], [G]
Si-5	11.6	0.9	87.4	30	[G]
SiC	11.75	2.5	81.6	15	[V]
Si-6	12.5	0.7	81.5	30	[G]
Ne-II	12.81	0.2	63.3	15	[V], [G]
Ne-II (ref2)	13.1	0.2	67.4	15	[V], [G]
QH2	17.0	0.4	46.1	15	[V]
Q1	17.65	0.9	57.9	15	[V]
Q4	20.5	1.0	59.0	15	[V]
Q8	24.5	0.8	55.8	15	[V]
Qwide	20.9	8.8	~72%	30	[G], Spectroscopic Blocker

[V] Part of VISIR consortium (VISIR=VLT Mid Infrared Spectrometer/Imager; see http://www.eso.org/instruments/visir/)
[G] Similar filter available in Gemini's mid infrared imagers/spectrometers T-ReCS and Michelle (see http://www.gemini.edu/sciops/instruments/michelle/MichIndex.html)

2.7 Slit Wheel

Eleven positions, one of which is clear (open) and another blank, are available in the slit wheel. The nine remaining positions are populated with slit masks for use in the 10 and 20 μm spectroscopic modes (see Table 7). All slits are 16 mm in length, spanning the entire short dimension of the detector. The slit widths were selected to cover a range of seeing conditions, from diffraction limited at the shortest wavelength of the N band window to 1.04”. For additional blocking, the slit dekker in the aperture wheel can be used as a very oversized ‘slit’, but in laboratory tests this was not needed. The slit parameters are listed in Table 7.

Table 7 Slit Wheel Positions

Slit Width [arcsec]	10μm Diffraction Limited Central λ [μm]
Blank	-
0.17	7.0
0.20	8.3
0.23	9.5
0.26	10.7
0.36	14.9
0.41	16.9
0.45	18.6
0.52	21.5
1.04	Seeing limited
Open	Used in Imaging

2.8 Wollaston Prism Slide

The Wollaston prism maybe inserted into the optical beam to permit polarimetric observations (in conjunction with the HWP), or to insert the ‘flip-mirror’ (see grating turret section below). In all other modes, the slide is moved to the open position, thereby giving this mechanism three positions of operation. More details about the Wollaston and issues concerning CanariCam polarimetry are discussed as part of the polarimetry data reduction section at the end of this document.

Table 8 Wollaston Slide Positions

Position	Description
Clear	Wollaston and mirror out of beam for all standard observing modes
Mirror	Flip mirror in the beam (see grating turret below)
Wollaston	Wollaston in the beam for polarimetric observations

2.9 Mirror & Grating Turret

The grating turret provides the main mirror for all science imaging, and four gratings for the spectroscopy modes. The turret utilizes a single stepper motor, which may rotate into the science beam any of the following five components: imaging mirror, low resolution 10 μm grating, high resolution 10 μm grating, low resolution 20 μm grating, high resolution 20 μm grating (Table 9). When using the high-resolution gratings, the grating may be positioned to center any wavelength within the operating range on the detector array. Multiple settings of the high-resolution gratings are needed to span the entire 10 or 20 μm atmospheric window. When using either of the low-resolution gratings, a single setting places the entire operational wavelength range for that grating on the detector array. The gratings are optimized for use in first order, and are gold-coated master gratings on aluminum substrates. While using CanariCam in the spectroscopic mode, it may be desirable to monitor the source location in the slit; the source position may drift due to, for example, telescope tracking errors, differential refraction, and flexure. This is simply and readily achieved with the use of the 'flip-mirror' located on the Wollaston prism slide (see above). The procedure to confirm the source position with respect to the slit is to set the instrument for standard spectroscopic observations, and then use the flip mirror to divert the beam before it reaches the grating. Although the resultant image is somewhat vignetted and aberrated (the optical path with flip mirror inserted deviates from the optimum path), the source location is still indicated adequately. Once this confirmation has taken place, the flip mirror is retracted and normal observations continued.

Some non-repeatability in the positioning of the grating turret can occur, so one should confirm the position of the grating with care before starting observations. In the low-resolution modes, the dispersion in the N and Q windows is such that light will never be dispersed beyond the array even if there is a slight error in the turret position, which, however, may vary from night to night. This does not pose a problem for the data reduction, but one should still be aware of this possibility. The positional repeatability of the gratings and main imaging mirror can be seen in Table 10,which shows the mean one-sigma error.

Table 9 Grating Wheel Positions

Grating Wheel Position	Description
Mirror	Mirror position for imaging
LowRes-10	10 μm low resolution grating
LR_Ref_Mirror	Reference mirror for LowRes-10 and LowRes-20 grating
LowRes-20	20 μm low resolution grating
HighRes-10	10 μm high resolution grating
HR_Ref_Mirror	Reference mirror for HighRes-10 grating

Table 10 Mirror and Grating Repeatability

Grating Wheel Position	σ_x [pixel]	σ_x [arcsec]
Datum to Imaging	3.6	0.288

Position to Position	0.2	0.016

The grating properties are summarized in Table 11. The spectral resolution R ≡ λ/Δλ applies to the central wavelength of the grating, with the use of a slit of width λ_{max}/D, where λ_{max} is the maximum wavelength accessible to the grating (13.5 μm for the LoRes-10 and HiRes-10 gratings and 26 μm for the LoRes-20 grating), and D (= 10.4 m) is the telescope aperture diameter. The predicted resolutions for the low-resolution gratings are shown in Table 11. The resolution of the HiRes-10 grating is limited to R < 1260 by the 15 mm pupil image near the position of the gratings.

Because of the dispersion of the high-resolution grating (Δλ = 0.01 μm), only about 1 μm can be observed on the array at one time. In order to cover different wavelength regions within the atmospheric window, the angle of the high-resolution grating is changed by rotating the grating turret.

Table 11 Grating Parameters

	LowRes-10	LowRes-20	HighRes-10	HighRes-20
Central Wavelength (λ_{center}) (µm)	10.5	20.5	10.5	20.5
Slit width (λ_{max}/D)	0.28”	0.53”	0.28”	0.53”
Blaze λ (µm)	9.87	19.96	10.08	20.18
Blaze Angle (°)	2.6	4.0	16.4	20.8
Lines mm^{-1}	9.1	6.1	56.0	35.2
$\Delta\lambda_{Detector}$ (µm)	6	9	0.98	1.54
Incidence Angle (°)	14.8	15.7	29.5	33.7
Diffraction Angle (°) at λ_{center}	9.2	8.3	5.5	9.7
R=λ/Δλ	175	120	1313	891
Smallest Resolvable λ (µm)	0.06	0.17	0.008	0.025

3 Software Operation: Queue and Classical Observing

Software associated with normal observing using CanariCam is provided by the GTC Observatory. This will include the observation request (bidding for time, phase 1) and the detailed manner in which the observations should be executed (the observing tool, phase 2). CanariCam will have two primary styles of observing – classical or service (analogous to queue) observing. We discuss the two styles below:

1. Classical. This is the traditional type of observing, where the astronomer visits the telescope and executes the observations with help from the observatory staff. Data is taken in the conditions at that moment, and no observatory attempt is made to match the type of observations to the prevailing conditions. If the weather is unsuitable for CanariCam observations, it maybe possible to switch to another instrument, but this is wholly dependant on GTC rules and regulations. We note that MIR observations typically require demanding observing conditions and it is our experience that classical observing is an often poor way to collect MIR data. Phase 1 and 2 are still needed to be completed, and depending on GTC rules and regulations, changes to the phase 2 targets and/or observation mode may be disallowed.
2. Service (or queue). In this observing style the phase 2 program is executed by observatory staff without further contact with the principal investigator. The observations are executed only when observing conditions at that time meet with the principal investigator's requirements. Data is provided to the principal investigator through a ftp-based retrieval system. Implicit in this type of observing is that no visiting observers visit the observatory, rather the observations are made by the expert GTC staff astronomers.

The two styles of observations demand slightly different capabilities from the principal investigator. This document contains all the information needed for the service observer. For the classical observer, the person should have read and understood this document as well as the software document. For descriptions and help using such software see your local GTC staff. Software such as the Java CanariCam Interface (JCI) and the Java Display Device (JDD) as well as software architecture details are described in the CanariCam Software Manual. The standard classical-based user should consult document CTRD-2, the CanariCam control system operator manual for JCI and JDD.

4 Observing and Data Reduction

4.1 Introduction

In this section, we discuss the CanariCam data structure, additional comments on chopping and nodding, observational planning, specific comments on polarimetry, and then the subsequent data reduction. In all the sections below, a working version and knowledge of both IRAF and Starlink software suites is assumed, and internet access to the Gemini mid-IR resources pages is essential. We note the outstanding work of the Gemini mid-IR team, and we make substantial use of their results. The key people associated with those activities are Drs. Rachel Mason, Kevin Volk, and Scott Fisher. We also use sections of the Starlink POLPACK software, written and documented by Berry & Gledhill. Much of the IRAF script work for the software was written by, or under the direction of, Kathleen Labrie, also at Gemini.

We assume that the user has:

1. A Unix-based computer;
2. A working knowledge of IRAF (essential), with a working knowledge of Starlink also being desirable;
3. The Gemini version of IRAF (version 1.9.1) **tested and running**. The package can be downloaded from: http://www.gemini.edu/sciops/data-and-results/processing-software
4. Starlink software, version Humu (Altair) **tested and running**. The package can be downloaded from: http://starlink.jach.hawaii.edu/

4.2 Chopping & Nodding

It is generally believed that we chop (i.e., oscillate at several hertz) the telescope secondary mirror wholly to account for the time variable sky background and/or transmission. While the sky variation can be significant, one must make chopped observations even for perfect sky conditions, due to the so-called 1/f ("one over f") noise that is common to mid-IR arrays. The 1/f noise arises from electronic noise within the array and associated circuitry, and hence is intrinsic. Each array has a characteristic frequency distribution of noise. Furthermore, the closed cycle cooler which keeps the array cool enough for science operation produces a noise spike at ~1 Hz. Thus, the chop frequency is a carefully selected value based on both the array characteristics and typical sky conditions.

4.3 CanariCam Data Structure & Exposure Times

CanariCam data is delivered in standard multi-extension FITS (MEF) file format. Each extension contains the 320x240 pixel image, as well as specific headers relevant to those extensions. The zeroth header is a general header, containing greater information about the full data file.

When CanariCam is setup for engineering modes or unusual observing modes, the instrument/GTC may not use chopping (and thus would not nod). In this case, the images are stored as [320,240,1,N] where N is the number of savesets. Savesets are automatically defined by the CanariCam software to optimize for observing efficiency and full-well depth, and can be adjusted for specific observing routines, but this is rarely needed. A typical imaging frame time is ~25 ms, and a saveset time is ~10 s.

In chop and chop-nod modes, there are 2 chop positions per saveset, and M savesets, meaning that each image is therefore [320,240,2,M]. Almost all science data are taken in chop-nod mode, and each extension contains the savesets for a single nod position. CanariCam can be used in the nod sequences ABAB or ABBA, with the difference being only an insignificant change in overheads. However, it is essential for a minimum number of AB pairs to be observed to permit adequate correction for radiative offset (see appendix below for a detailed explanation of the reasons for chopping and nodding).

The exposure time can be a confusing term when applied to mid-IR observations, there are four exposure time commonly expressed:

1. Frame time. This is the time between readouts of the array and is controlled through the optimized software settings. Typical times are ~25 ms.
2. Saveset time. This is the time between each co-added dataset that is saved to disc. This is the smallest quantum of data saved by CanariCam. This is controlled through the optimized software settings. Typical times are ~10 s.
3. Exposure time. This is the user-selected time interval over which the source will be observed. The time can vary greatly depending on source flux, but typically it is in the range ~60-600s.
4. Clock (or total) time. This is the total time need for the observation to be completed, and includes the necessary overheard of chopping and nodding. The multiplicative factor to convert exposure time to clock time is dependant on the observing mode, chop and other parameters used, but is estimated to be ~3 for imaging, ~4 for spectroscopy and ~3.75 for imaging polarimetry.

Thus, a typical dataset may consist of 25-ms frames, of 10-s savesets, with a 600-s exposure time, which results in a clock time of 1800-s. It is important to note that only the exposure time is input by the user. All other parameters are set automatically, although the typical user would usually monitor the exposure times and clock times. Because the exposure time is built from units of frametime, and there must be an even number of chop/nods as well as certain values for some other system parameters, it works out that only certain discrete values for the exposure time are permissable. Therefore, the CanariCam observing software adjusts the exposure time slightly to the next longest value that fits the set of time constraints.

4.3 CanariCam Filters and Calibration Objects

The CanariCam filter set spans the 10 and 20 μm atmospheric windows. Spectrally broad (>>1μm), medium (~1μm) and narrow (~0.1μm) filters are available, offering a versatile imaging suite of filters. The 10 μm window is far 'cleaner' (high transparency with few absorption bands) than the 20 μm window. However, even the 10 μm window suffers from a strong and highly variable absorption band from O_3 (Ozone) centered at 9.7 μm. In both atmospheric windows, the atmospheric absorption band(s) increase the photon 'noise' and can degrade the final signal-to-noise ratio of the images. Interestingly, in the case of the N-band filter, it has been shown on-sky that the intermediate bandwidth filters of the silicate set (Si1-6) have similar sensitivities to the broadband filter. When using the Si filters, one can gain two key advantages over and above the N band filter:

1. The flux is from a more constrained wave band;

2. If using a Si filter with a shorter λ_c than the approximate λ_c of the N-band filter, the diffraction limit is smaller, providing higher–spatial-resolution images.

Further considerations of filter selection include the sensitivity of the filter and the source color through the mid-IR windows, which bears on system sensitivity (e.g. flux standards are often blue and can be very difficult to observe at long wavelengths), flux calibration (a strong color through the filter should be corrected for), and PSF corrections (a blue object will have a smaller observed FWHM than a red object of the same true width when observed through a filter with a finite filter width).

The seeing at mid-IR wavelengths is much better than at optical and near-IR wavelengths, with mid-IR imaging being typically at or near the diffraction limit (~0.25" at N, ~0.5" at Q). With good seeing and good telescope performance, 2-3 Airy rings can be observed around a bright object. Typical recorded Strehl ratios at Gemini are ~0.6 at N and ~0.9 at Q.

When imaging, two calibrators are typically required, one to monitor the point-spread function (PSF) and one to establish the flux. Typically these are two different sources, because the flux standard, which is bright, is usually located far from the science source on the sky, whereas the PSF star must be relatively close to the program source. It is important to observe the PSF standard as close in time and telescope slew as the science object to minimize the change of gravity vector, pupil rotation and temporal changes of the PSF.

There are relatively few flux standards available for use with 8-10-m class telescopes, since many standards saturate when observed with these large apertures. Flux standards are typically drawn from one of the following lists:

- Primary or secondary 'Cohen' standards;
- Very bright southern standard stars, but many of these sources may saturate CanariCam/GTC unless there is a telescope defocus.

The Cohen standards are developed from models of continuous spectra of many stars tied carefully to observational data. These model spectra can be used for imaging and spectroscopic flux calibration by integrating over the filter bandpass or smoothing to the appropriate spectral resolution. A detailed discussion of this work can be found in Cohen et al. 1999, AJ, 117, 1864, but we note here that the calibration is anchored to two primary standard, Alpha Lyr (A0 V) and Alph CMa (A1 V). Gemini has some outstanding tools to assist with this procedure: see http://staff.gemini.edu/~kvolk/brightness.html which calculates the estimated fluxes for the filters fitted in T-ReCS and Michelle. We note that airmass corrections at mid-IR wavelengths are not usually done unless large blocks of time are available for a specific program to permit observations over a broad range of airmasses. It is strongly recommended for programs that critically depend on accurate photometry that the flux calibrator be observed close in time and nearby on the sky to the science target.

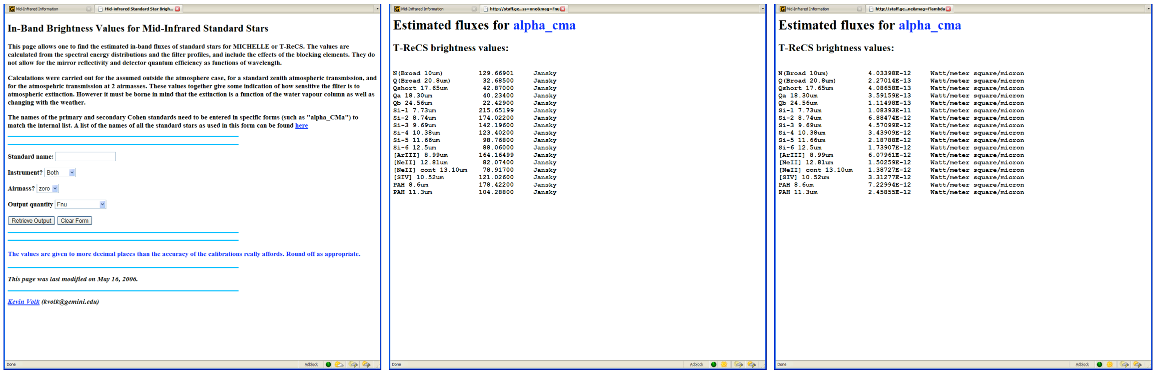

Figure 11. Gemini tools for in-band flux calibration.

Gemini also provides a useful tool for selecting flux standards: http://staff.gemini.edu/~kvolk/standard.html. This selects several stars close in time and space to the science object.

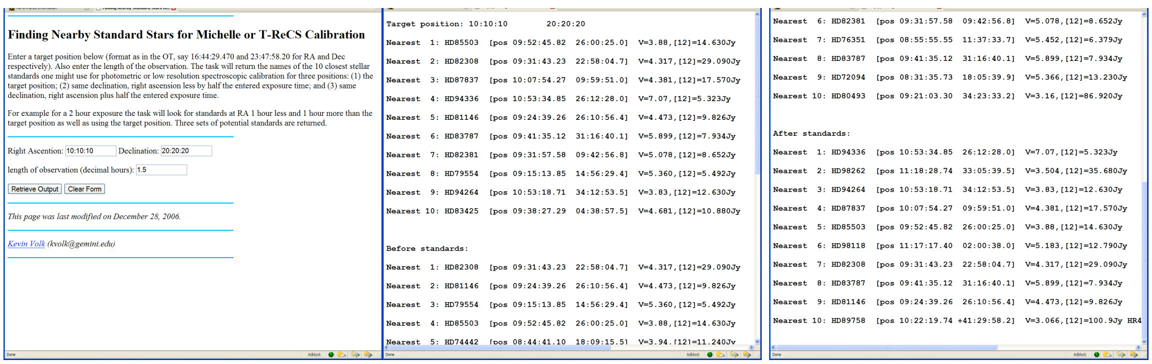

Figure 12. Gemini tools for flux standard selection.

PSF standards are observed to monitor the image quality of the telescope. We note that sometimes the flux standard can be used for PSF calibration, but that is the exception rather than the rule, since, as note above, in many cases the flux standard is too bright, too blue, or an unrepresentative color compared to the science source. The best PSF sources are giant stars of type K or M. Note that M supergiants are usually avoided due to possible extended dust shell emission, although they are sometimes useful secondary standards. Also, very bright stars should be avoided due to the array artifacts they cause. PSF stars can also be selected by using the Hipparcos on-line database. When using PSF standards and depending on the program goals, one may need to take into account pupil rotation inherent in any long-time observations or when slewing to other sources; the PSF widths at all brightness levels for a hexagonally-segmented mirror like GTC is a function of the PSF azimuth.

Although mid-IR observations are often at or near the diffraction limit, seeing can degrade and deform the image quality. The image below shows a long-term observation at 8.8 μm of the AGN (solid circles) at the center of Centaurus A (Radomski et al. 2008) and the associated PSF object (open circles). The PSF is clearly variable. If, as is commonly the case, the PSF standard is much bluer than the science source, and a wide bandpass is used, a color correction may need to be made. In the extreme case of comparing a blue 10,000 K star to that of a 50 K source, the FWHM correction for observations through the broadband N filter is 25.5%

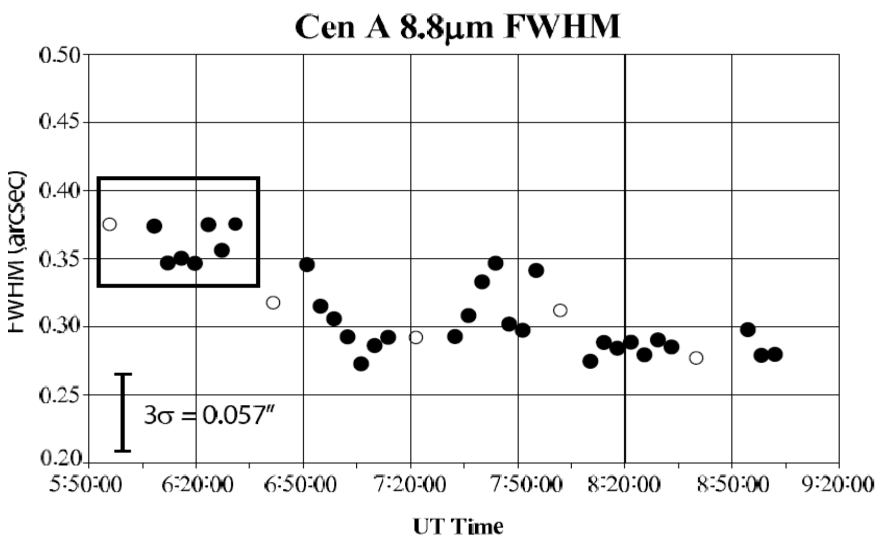

Figure 13. Variation of the FWHM vs. time (Radomski et al 2008).

4.3 CanariCam Imaging Data Reduction

The standard tool for CanariCam data reduction is the IRAF data reduction package, and the Gemini tools (found at http://www.gemini.edu/sciops/data-and-results/processing-software) must be installed and operational. In the future, IRAF will evolve to pyraf, and the data reduction tools will be ported to that platform.

The imaging data reduction consists of five main tasks, or combined in one meta-task, listed and considered below:

- TBACKGROUND
- TPREPARE
- TVIEW
- MISTACK
- MIREGISTER

And the meta-task:

- MIREDUCE

4.3.1 TBACKGROUND

This task is used to derive statistics on the background flux for each of the chop saveset. Compromised savesets with obviously high noise can be flagged to 'bad', and thereby excluded from inclusion in the data reduction. The data can be compromised due to:

- Clouds
- Poor-seeing and/or guiding
- Enhanced water vapor
- Increased noise

The screenshot below of the EPAR of TBACKGROUND shows the input parameters, with the key parameter being the sigma tolerance for bad frames. Whilst this task can be useful, as is common with automatic tasks, it can be error prone. Instead, it is preferable to use TVIEW to investigate, by hand, the images where possible.

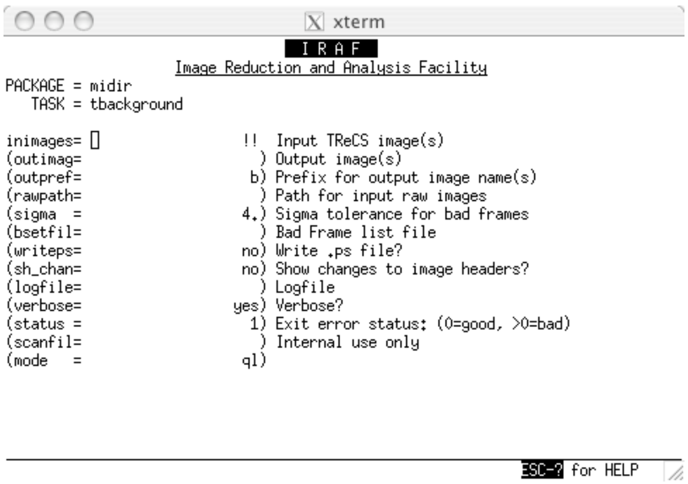

```
xterm
                              I R A F
                Image Reduction and Analysis Facility
PACKAGE = midir
   TASK = tbackground

inimages=                    !!  Input TReCS image(s)
(outimag=                      ) Output image(s)
(outpref=                     b) Prefix for output image name(s)
(rawpath=                      ) Path for input raw images
(sigma  =                    4.) Sigma tolerance for bad frames
(bsetfil=                      ) Bad Frame list file
(writeps=                    no) Write .ps file?
(sh_chan=                    no) Show changes to image headers?
(logfile=                      ) Logfile
(verbose=                   yes) Verbose?
(status =                     1) Exit error status: (0=good, >0=bad)
(scanfil=                      ) Internal use only
(mode   =                    ql)

                                                   ESC-? for HELP
```

Figure 14. EPAR of TBACKGROUND.

4.3.2 TPREPARE

This task is used only to reformat the data for some of the later scripts and user manipulation. Since production of TPREPARE, most tasks do not require its use and hence we do not consider this task further.

4.3.3 TVIEW

This task is used to display the savesets to the display of choice (e.g. ds9) to allow investigation of the images. This can be done automatically, where the images are automatically displayed to the image tool, or interactively, where image parameterization can be performed using IMEXAM. After examination in interactive mode, nods can be flagged as ‘bad’ and excluded in subsequent data reduction. As there must be an ‘even’ number of nod positions, TVIEW ensures the output file achieves this.

```
xterm
I R A F
Image Reduction and Analysis Facility
PACKAGE = midir
   TASK = tview

inimages= S20040201S0118.fits  Input T-ReCS image(s)
(outimag=                    ) Output image(s)
(outpref=                   v) Prefix for output image name(s)
(rawpath=                    ) Path for input raw images
(type   =                 dif) Type of frame (src|ref|dif)
(delay  =                  0.) Update delay in seconds
(fl_inte=                 yes) Interactive screening of frames?
(fl_disp=                  no) Fill display
(fl_labe=                 yes) Label display
(colour =               black) Label colour: black|white|red|green|blue|yellow
(fl_use_=                  no) Use imexam to look at images before screening?
(fl_sh_c=                  no) Show changes to image headers
(fl_dele=                 yes) Delete unchanged copy images
(z1     =                  0.) Minimum level to be displayed
(z2     =                  0.) Maximum level to be displayed
(zscale =                 yes) Display graylevels near the median
(zrange =                 yes) Display full image intensity range
(ztrans =              linear) Greylevel transformation (linear|log|none|user)
(logfile=                    ) Logfile name
(verbose=                 yes) Verbose
(status =                   0) Exit status: (0=good, >0=bad)
(scanfil=                    ) Internal use only
(mode   =                  ql)

                                                     ESC-? for HELP
```

Figure 15. EPAR of TVIEW.

4.3.4 MISTACK

This task collapses the full data set (minus any 'bad' flagged data) into a single [320,240] MEF, where extension 0 is the header, and 1 is the image. The user can select if the data is co-added or co-averaged. This is the most commonly used manner to reduce MIR data.

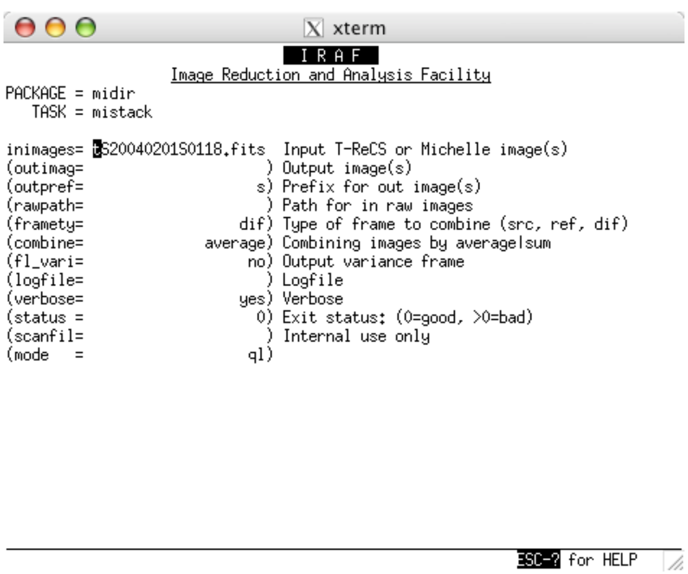

```
xterm
I R A F
Image Reduction and Analysis Facility
PACKAGE = midir
   TASK = mistack

inimages= S20040201S0118.fits  Input T-ReCS or Michelle image(s)
(outimag=                    ) Output image(s)
(outpref=                   s) Prefix for out image(s)
(rawpath=                    ) Path for in raw images
(framety=                 dif) Type of frame to combine (src, ref, dif)
(combine=             average) Combining images by average|sum
(fl_vari=                  no) Output variance frame
(logfile=                    ) Logfile
(verbose=                 yes) Verbose
(status =                   0) Exit status: (0=good, >0=bad)
(scanfil=                    ) Internal use only
(mode   =                  ql)

                                                     ESC-? for HELP
```

Figure 16. EPAR of MISTACK.

4.3.5 MIREGISTER

This task collapses the full data set (minus any 'bad' flagged data) into a single [320,240] MEF, where extension 0 is the header, and 1 is the image. The user can select if the data is co-added or co-averaged. The difference between MIREGISTER and MISTACK is the invocation of the XREGISTER task of IRAF to shift the images to a common peak of a source before co-addition or co-averaging. This task requires a bright point-source in each of the savesets for reliable operation and hence the MISTACK task is more commonly used than MIREGISTER.

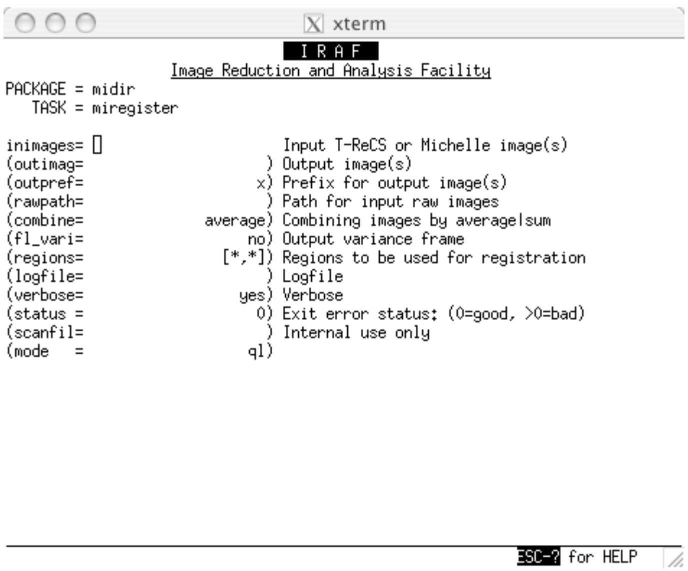

```
xterm
                                 I R A F
                    Image Reduction and Analysis Facility
PACKAGE = midir
   TASK = miregister

inimages=                         Input T-ReCS or Michelle image(s)
(outimag=                       ) Output image(s)
(outpref=                      x) Prefix for output image(s)
(rawpath=                       ) Path for input raw images
(combine=                average) Combining images by average|sum
(fl_vari=                     no) Output variance frame
(regions=                  [*,*]) Regions to be used for registration
(logfile=                       ) Logfile
(verbose=                    yes) Verbose
(status =                      0) Exit error status: (0=good, >0=bad)
(scanfil=                       ) Internal use only
(mode   =                     ql)

                                                        ESC-? for HELP
```

Figure 17. EPAR of MIREGISTER.

4.3.5 MIREGISTER

This task calls most of the previous packages in a non-interactive manner, and is the easiest, most automated and most commonly used manner to reduce data. The task calls TPREPARE, MISTACK or MIREGISTER, and can call TVIEW and TBACKGROUND if those flags are set to true. The output file is a 320x240 pixel file in the 1st extension, whose 0th extension is the full FITSHEADER. Once the data is in this format, manipulation and measurements can be performed using standard FITS tools and/or packages.

4.4 CanariCam Spectroscopy Data Reduction

In this section we discuss mid-IR spectroscopy preparation and data reduction. We explain the methods for taking raw data and producing a flux and wavelength calibrated spectrum. As with the imaging data above, the Gemini mid-IR IRAF package is key to accomplishing this goal, and we are particularly indebted to the Gemini staff who wrote the "MIR resources" Gemini WWW pages, especially Kevin Volk, Rachel Mason and

Scott Fisher. The section will concentrate on the msreduce package, which can be used with:

- The single spectrum of an object, and resulting in a wavelength calibrated spectrum;
- Two spectra (source and telluric standard), and resulting in a wavelength and flux calibrated spectrum

Implicit in the above is that two spectra are observed, one for the object and the second for calibration. Flat fields are often taken, but are unimportant for compact sources. For the calibration source, a star or asteroid are often used. Asteroids are preferable when using higher spectral resolution as some stars can show resolvable spectral features. At lower spectral resolution stars are often better, since one can use these objects as both flux and wavelength calibrators.

Telluric standards are used to remove effects of atmospheric transmission. Based on experience on Cero Pachon and Mauna Kea, for objects observations lasting >30 minutes (elapsed time), two telluric standards are suggested, post and prior to observing. In the case of Gemini, one of those is 'free'. At low spectral resolution, B, A, F and G type stars have a smooth spectrum in the mid-IR region, and K and M type stars should be avoided. For a list of B-G type stars, see the compilation at the Gemini mid-IR resources WWW site (http://www.gemini.edu/sciops/instruments/mir/MIRSpecStdBAFG.html) and a screen shot of which is shown below.

MIR@gemini

Bright Stars with Spectral Types B-G

A list of bright telluric standard stars of spectral types B-G for calibration of Michelle spectra is provided below, along with **estimated** (in most cases) magnitudes at N and Q. Note the following restrictions on use of the stars in the list below.

- At low resolution B, A, F, and G stars have smooth spectra in the 7-25um region, and therefore all may be used to correct for atmospheric absorption features. At moderate resolution G stars also should be avoided, but B-F stars are OK. At high resolution only B and early A stars are suitable (except for measuring hydrogen lines).
- All of the stars in the list are bright enough to obtain good S/N lowN grating spectra in reasonably short integrations.
- For medN1 spectra, only the stars brighter than ~1st magnitude are bright enough.
- For medN2 and lowQ spectra, only the stars brighter than ~0th magnitude are bright enough.
- For echelle spectra, only Sirius (BS 2491) is bright enough; asteroids almost always must be used.

HR/BS	RA (2000)	Dec	V	Sp	N & Q (est) * ==> existing photometry
1713	5:14:32.27	-8:12:05.9	0.12	B8Iab	0.0
1791	5:26:17.51	+28:36:26.8	1.68	B7III	1.7
2618	6:58:37.55	-28:58:19.5	1.51	B2Iab	2.0
3982	10:08:22.31	+11:58:01.9	1.35	B7V	1.6
5056	13:25:11.58	-11:09:40.8	1.04	B1III-IVD	1.6
6879	18:24:10.32	-34:23:04.6	1.80	B9.5III	1.6
2421	6:37:42.70	+16:23:57.3	1.90	A0IV	1.8
2491	6:45:08.92	-16:42:58.0	-1.47	A1V	N=-1.42*, Q=1.36*
2891	7 34 35.9	+31 53 18	1.58	A1VD	1.6
4534	11 49 03.58	+14 34 19.4	2.14	A3V	N=1.84*, Q=1.83*
4905	12 51 50.08	+56 13 51.2	1.76	A0p	1.7
5793	15 32 34.14	+26 52 54.7	2.21	A0V	N=2.19*, Q=2.04*
6556	17 34 56.07	+12 33 36.1	2.10	A5III	1.5
7001	18 36 56.34	+38 47 01.3	0.00	A0V	N=0.00*, Q=0.00
7557	19 50 47.00	+08 52 06.0	0.77	A7V	0.2
7924	20 41 25.91	+45 16 49.2	1.25	A2Iae	0.8
8728	22 57 39.05	-29 37 20.1	1.16	A3V	1.1
1017	3 24 19.37	+49 51 40.2	1.82	F5Iab	0.4
1543	4 49 50.41	+06 57 40.6	3.19	F6V	2.0
1865	5 32 43.82	-17 49 20.2	2.60	F0Ib	1.6
2693	7 08 23.48	-26 23 35.5	1.84	F8Iab	0.2
2943	7 39 18.12	+05 13 30.0	0.34	F5IV-V	N=-0.76*, Q=-0.73*
3775	9 32 51.43	+51 40 38.3	3.20	F6IV	1.9
6553	17 37 19.13	-42 59 52.2	1.86	F1II	0.7
6615	17 44 05.10	-40 06 34.9	3.02	F2Iae	1.8
7264	19 09 45.83	-21 01 25.0	2.89	F2II/III	1.7
7796	20 22 13.70	+40 15 24.0	2.24	F8Iab	0.3
437	1 31 29.01	+15 20 45.0	3.63	G7IIa	1.4
509	1 44 04.08	-15 56 14.9	3.50	G8V	1.6
510	1 45 23.63	+09 09 27.8	4.27	G8III	2.0
854	2 54 15.46	+52 45 44.9	3.94	G4III+A4V	1.9
915	3 04 47.79	+53 30 23.2	2.95	G8III+A2V	1.0
1030	3 24 48.79	+09 01 43.9	3.62	G6III	1.5
1195	3 49 27.25	-36 12 00.9	4.17	G9II-III	1.9
1409	4 28 37.00	+19 10 49.6	3.54	G9.5III	1.1
1464	4 35 33.04	-30 33 44.4	3.82	G8III	1.5
1708	5 16 41.36	+45 59 52.8	0.08	G5III	N=-1.94*, Q=-1.93*
1784	5 23 56.83	-07 48 29.0	4.14	G8III	1.8

Figure 18. Suitable stars of type B-G taken from the Gemini WWW site.

The Gemini MIR resources page also provides an automated script to suggest optimal spectroscopic calibration stars. This is linked below, and the screen shot below shows the input and output from the script. Note that many of the standards are so-called Cohen standards, as they are drawn from Cohen's seminal work on standards.

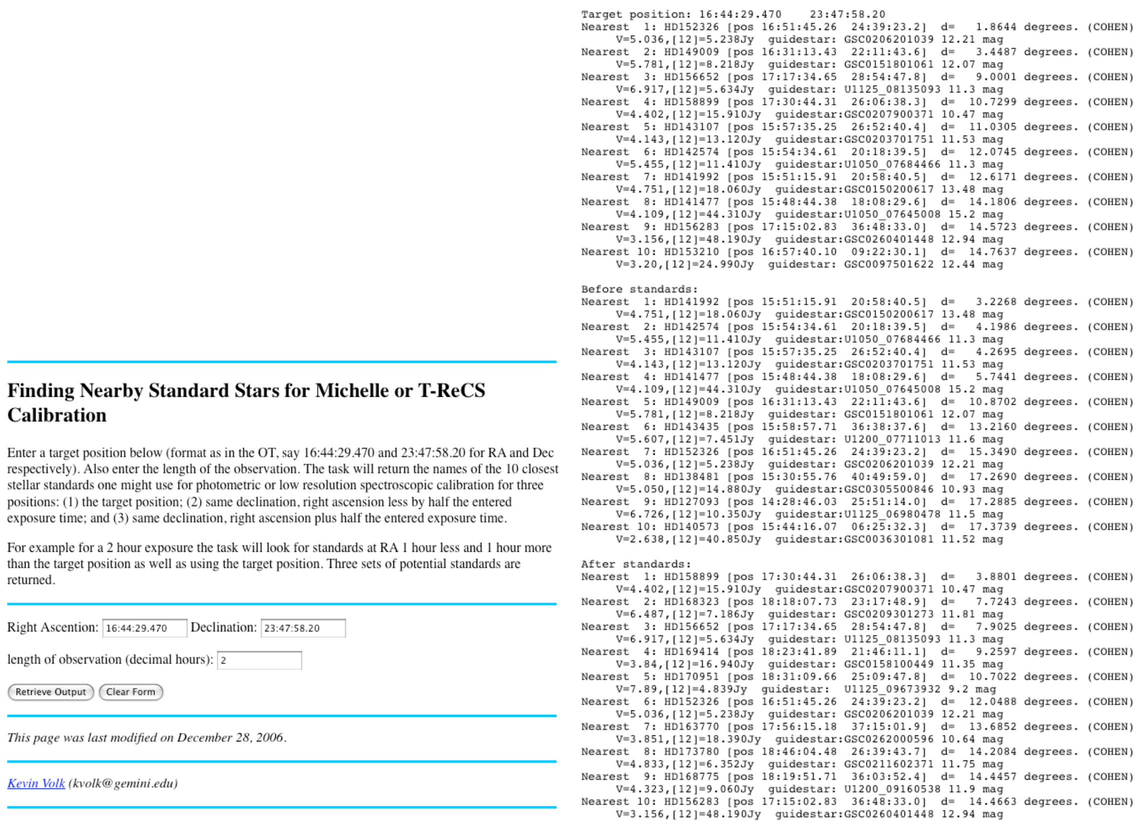

Finding Nearby Standard Stars for Michelle or T-ReCS Calibration

Enter a target position below (format as in the OT, say 16:44:29.470 and 23:47:58.20 for RA and Dec respectively). Also enter the length of the observation. The task will return the names of the 10 closest stellar standards one might use for photometric or low resolution spectroscopic calibration for three positions: (1) the target position; (2) same declination, right ascension less by half the entered exposure time; and (3) same declination, right ascension plus half the entered exposure time.

For example for a 2 hour exposure the task will look for standards at RA 1 hour less and 1 hour more than the target position as well as using the target position. Three sets of potential standards are returned.

Right Ascention: 16:44:29.470 Declination: 23:47:58.20

length of observation (decimal hours): 2

Retrieve Output Clear Form

This page was last modified on December 28, 2006.

Kevin Volk (kvolk@gemini.edu)

```
Target position: 16:44:29.470    23:47:58.20
Nearest  1: HD152326 [pos 16:51:45.26  24:39:23.2]  d=   1.8644 degrees. (COHEN)
     V=5.036,[12]=5.238Jy  guidestar: GSC0206201039 12.21 mag
Nearest  2: HD149009 [pos 16:31:13.43  22:11:43.6]  d=   3.4487 degrees. (COHEN)
     V=5.781,[12]=8.218Jy  guidestar: GSC0151801061 12.07 mag
Nearest  3: HD156652 [pos 17:17:34.65  28:54:47.8]  d=   9.0001 degrees. (COHEN)
     V=6.917,[12]=5.634Jy  guidestar: U1125_08135093 11.3 mag
Nearest  4: HD158899 [pos 17:30:44.31  26:06:38.3]  d=  10.7299 degrees. (COHEN)
     V=4.402,[12]=15.910Jy  guidestar:GSC0207900371 10.47 mag
Nearest  5: HD143107 [pos 15:57:35.25  26:52:40.4]  d=  11.0305 degrees. (COHEN)
     V=4.143,[12]=13.120Jy  guidestar:GSC0203701751 11.53 mag
Nearest  6: HD142574 [pos 15:54:34.61  20:18:39.5]  d=  12.0745 degrees. (COHEN)
     V=5.455,[12]=11.410Jy  guidestar:U1050_07684466 11.3 mag
Nearest  7: HD141992 [pos 15:51:15.91  20:58:40.5]  d=  12.6171 degrees. (COHEN)
     V=4.751,[12]=18.060Jy  guidestar:GSC0150200617 13.48 mag
Nearest  8: HD141477 [pos 15:48:44.38  18:08:29.6]  d=  14.1806 degrees. (COHEN)
     V=4.109,[12]=44.310Jy  guidestar:U1050_07645008 15.2 mag
Nearest  9: HD156283 [pos 17:15:02.83  36:48:33.0]  d=  14.5723 degrees. (COHEN)
     V=3.156,[12]=48.190Jy  guidestar:GSC0260401448 12.94 mag
Nearest 10: HD153210 [pos 16:57:40.10  09:22:30.1]  d=  14.7637 degrees. (COHEN)
     V=3.20,[12]=24.990Jy  guidestar: GSC0097501622 12.44 mag

Before standards:
Nearest  1: HD141992 [pos 15:51:15.91  20:58:40.5]  d=   3.2268 degrees. (COHEN)
     V=4.751,[12]=18.060Jy  guidestar:GSC0150200617 13.48 mag
Nearest  2: HD142574 [pos 15:54:34.61  20:18:39.5]  d=   4.1986 degrees. (COHEN)
     V=5.455,[12]=11.410Jy  guidestar:U1050_07684466 11.3 mag
Nearest  3: HD143107 [pos 15:57:35.25  26:52:40.4]  d=   4.2695 degrees. (COHEN)
     V=4.143,[12]=13.120Jy  guidestar:GSC0203701751 11.53 mag
Nearest  4: HD141477 [pos 15:48:44.38  18:08:29.6]  d=   5.7441 degrees. (COHEN)
     V=4.109,[12]=44.310Jy  guidestar:U1050_07645008 15.2 mag
Nearest  5: HD149009 [pos 16:31:13.43  22:11:43.6]  d=  10.8702 degrees. (COHEN)
     V=5.781,[12]=8.218Jy  guidestar: GSC0151801061 12.07 mag
Nearest  6: HD143435 [pos 15:58:57.71  36:38:37.6]  d=  13.2160 degrees. (COHEN)
     V=5.607,[12]=7.451Jy  guidestar: U1200_07711013 11.6 mag
Nearest  7: HD152326 [pos 16:51:45.26  24:39:23.2]  d=  15.3490 degrees. (COHEN)
     V=5.036,[12]=5.238Jy  guidestar: GSC0206201039 12.21 mag
Nearest  8: HD138481 [pos 15:30:55.76  40:49:59.0]  d=  17.2690 degrees. (COHEN)
     V=5.050,[12]=14.880Jy  guidestar:GSC0305500846 10.93 mag
Nearest  9: HD127093 [pos 14:28:46.03  25:51:14.0]  d=  17.2885 degrees. (COHEN)
     V=6.726,[12]=10.350Jy  guidestar:U1125_06980478 11.5 mag
Nearest 10: HD140573 [pos 15:44:16.07  06:25:32.3]  d=  17.3739 degrees. (COHEN)
     V=2.638,[12]=40.850Jy  guidestar:GSC0036301081 11.52 mag

After standards:
Nearest  1: HD158899 [pos 17:30:44.31  26:06:38.3]  d=   3.8801 degrees. (COHEN)
     V=4.402,[12]=15.910Jy  guidestar:GSC0207900371 10.47 mag
Nearest  2: HD168323 [pos 18:18:07.73  23:17:48.9]  d=   7.7243 degrees. (COHEN)
     V=6.487,[12]=7.186Jy  guidestar: GSC0209301273 11.81 mag
Nearest  3: HD156652 [pos 17:17:34.65  28:54:47.8]  d=   7.9025 degrees. (COHEN)
     V=6.917,[12]=5.634Jy  guidestar: U1125_08135093 11.3 mag
Nearest  4: HD169414 [pos 18:23:41.89  21:46:11.1]  d=   9.2597 degrees. (COHEN)
     V=3.84,[12]=16.940Jy  guidestar: GSC0158100449 11.35 mag
Nearest  5: HD170951 [pos 18:31:09.66  25:09:47.8]  d=  10.7022 degrees. (COHEN)
     V=7.89,[12]=4.839Jy  guidestar:  U1125_09673932 9.2 mag
Nearest  6: HD152326 [pos 16:51:45.26  24:39:23.2]  d=  12.0488 degrees. (COHEN)
     V=5.036,[12]=5.238Jy  guidestar: GSC0206201039 12.21 mag
Nearest  7: HD163770 [pos 17:56:15.18  37:15:01.9]  d=  13.6852 degrees. (COHEN)
     V=3.851,[12]=18.390Jy  guidestar:GSC0262000596 10.64 mag
Nearest  8: HD173780 [pos 18:46:04.48  26:39:43.7]  d=  14.2084 degrees. (COHEN)
     V=4.833,[12]=6.352Jy  guidestar: GSC0211602371 11.75 mag
Nearest  9: HD168775 [pos 18:19:51.71  36:03:52.4]  d=  14.4457 degrees. (COHEN)
     V=4.323,[12]=9.060Jy  guidestar: U1200_09160538 11.9 mag
Nearest 10: HD156283 [pos 17:15:02.83  36:48:33.0]  d=  14.4663 degrees. (COHEN)
     V=3.156,[12]=48.190Jy  guidestar:GSC0260401448 12.94 mag
```

Figure 19. Automated standard star selection too, taken from the Gemini WWW site.

Many Cohen spectrophotometric standards are early K dwarfs, and many have accurate IRAS mid-IR flux densities, making them potentially good flux calibrators as well as telluric line removal stars. At low spectral resolution, the fundamental vibration-rotation band of SiO significantly depresses the spectrum at 7.5-10μm in stars later than around K0III – K2III. This can significantly affect the ratio'ing, but the effects can be removed or mitigated through use of a Cohen model template or through the Gemini IRAF msabsflux.

Any Cohen standard star can be used for both low spectral resolution N and Q band spectra. However, science programs that are aimed at detecting or measuring detailed shapes of weak spectral features in a strong continuum source in the N or Q band should use Cohen stars with care. At high spectral resolutions, the Cohen standards are unsuitable as telluric standards as they contain a multitude of photospheric absorption lines. Finally, we note that another set of Cohen standards, termed tertiary Cohen standards, are available, but these have not been well characterized observationally, and so their 'quality' as standards is generally unknown, and hence primary or secondary Cohen standards are recommended instead.

4.4.1 IRAF Reduction of Spectra

The spectroscopic equivalent of mireduce is called msreduce. There are two key ways to use this package: without or without executing telluric corrections through the use of the fl_standard flag. In this case, a wavelength calibrated raw spectrum is produced. If a flux standard is available, the spectrum can be reduced to provide a flux and wavelength calibrated spectrum, where the flux can be either to an absolute or relative scale. To start msreduce, the only parameter required is the object's raw data file name. Of course, if no telluric correction is needed, no standard spectrum is needed to be specified. Typically however, a standard is used, and the standard is defined by setting the fl_standard to yes. There are two possibilities set through flags if fl_standard is true:

a. If one sets the fl_blackbody flat to yes then the spectral shape of the calibration object will be assumed to follow that of a blackbody source
b. If a standard with a known spectrophotometric energy distribution (SED) is used for the telluric correction, the correction for both the atmospheric transmission and absolute flux level can be determined.

If absolute flux calibration is to be carried out, the name of the flux standard should be given in the stdname field. In the midir package, SED data for the TIMMI2 and a large set of Cohen standards is available. However, despite carefully following these steps, two uncertainties remain, that of slit losses (which are typically assumed to be the same for the objects as the standard star and hence ratio out) and that the calibration source is taken at a distance in zenith distance from the object and the sky transmission/emission may have changed between observing the two objects. Sky variation can be especially severe and rapid in the Ozone 9.7µm region of wavelength space.

If one uses the blackbody calibration routines, the resulting spectrum is of arbitrary flux scaling, and is normalized to 1 at a specific wavelength (11µm in the case of the low resolution N grating). In the case of an absolute spectrum, the units of the out are determined by the outtype parameter, where the default value is flux density in Jy.

In full detail, the steps of msreduce are as follows:

- Raw data can be corrected for the bias level and flat fielded using fl_flat, but this is rarely needed for CanariCam data
- The raw data files can be processed to provide stacked images for the sky and difference frames us fl_process
- Sky emission/absorption lines can then be used for wavelength calibration. It is generally necessary to check the initial identifications offered by the IRAF package even for low resolution spectra as the contrast between the lines and continuum is strongly dependant on the observing conditions. This is achieved using the fl_wavelength option.
- The wavelength calibration solution should then be applied to the entire field of view of the array using fl_transform.
- The spectrum can be defined and traced using the standard IRAF package nsextract, which in turns uses tasks from the apextract package by calling the fl_extract option.
- The spectrum is thus extracted into a wavelength calibrated raw spectrum.

- Should fringing be a problem, one can de-fringe the extracted spectra using fl_defringe.
- Finally, a telluric correction can be applied (using the fl_telluric command) and a final, wavelength and flux calibrated spectrum be output.

A flat field can be taken, should it be needed (for instance, if the object is observed on a substantially different position on the array from the calibration source) using a flat field screen in the sector wheel of CanariCam or of the diffuse sky or dome. Whilst typically not used, a bias frame can be obtained by placing all the CanariCam wheels into their blank position (where possible). In both cases, the observations are taken in stare mode, and hence the files only have one extension that contains either the flat or bias image. We note that the raw flat frame is a good approximation to that of a blackbody spectrum at the ambient temperature of the dome/instrument when the observation was taken. If the fl_flat flag is set to true, the names of the raw data files for the spectrum to be flat-fielded and bias frame subtracted must be defined as flat and bias. The msflatcor takes then takes these two files as input and creates a normalized flat, which in then applied to the science data by (1) subtracting off the bias level of the raw images and (2) dividing the resulting image by the normalized flat image. At the conclusion of this stage, an "f" is prefixed to the file name.

In the case of point sources, the flat fielding appears to make no appreciable difference to the resultant spectra. In the case of extended sources the flat field correction is *potentially* important, since the spectra of the source and standard may be observed at different parts of the array. In all cases, flat fielding of images is applied to the raw data files, before any stacking and differencing of the images is executed.

4.4.2 Initial Processing

This process takes the raw (or flat fielded) data, and carries out the initial processing required for all MIR data processing. The task is called using tprepare, or automatically called using the mistack task. For spectroscopy, one must stack the source frames in addition to make a sky spectrum images which is used for the wavelength calibration. Three output files are resultant from this step:

1. The prepared raw data file, prefixed with a "t'
2. The stacked difference file, prefixed with a "r"
3. The stacked sky spectrum file, prefixed with an "a"

4.4.3 Line IDs

This process identifies emission and/or absorption lines in the spectra for wavelength calibration. It typically needs to be accomplished in an interactive manner, as in most cases the lines marked automatically are incorrect. Wavelength calibration is accomplished using a sky spectrum, as arc spectra are not available in the N nor Q band. The nswavelength command is called, which in turn calls the gnris IRAF Gemini package, which in turn calls the identify NOAO IRAF package. The default N and Q band spectroscopic line IDs are in the data directory of the gnirs directory, but the "lines" can actually be blends or band features in some cases, such as in the case of the 9.503μm peak of the ozone feature, commonly used to calibrated the low resolution N band spectra. The extent to whish lines/bands are distinct from sky emission is a strong function of the conditions, and most especially the water vapor column along the line of sight, as well as the slit width used.

N-band λ (μm)	Q-band λ (μm)
7.467	17.586
7.875	18.298
8.514	18.648
8.802	19.015
9.503	19.310
10.260	19.890
11.728	20.322
12.877	20.653
	21.175
	21.855
	22.595
	22.941
	23.199

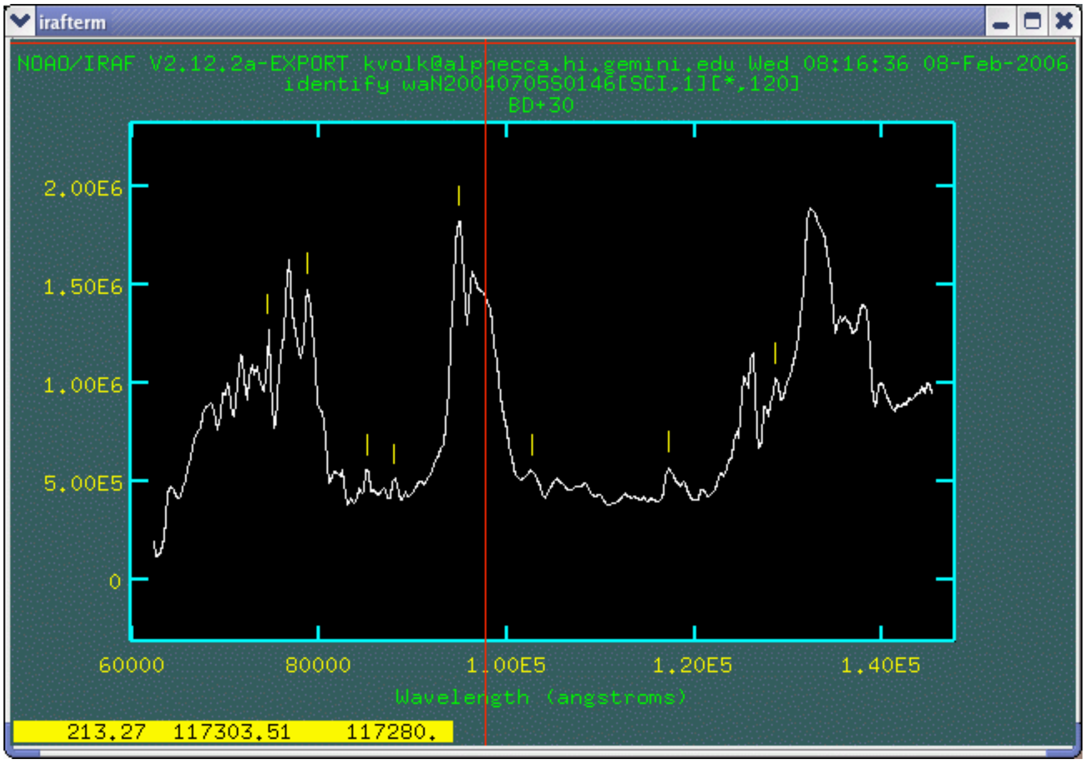

Figure 20. N band spectra during the line ID phase, using data taken in dry conditions with a narrow slit. Above the N and Q band line listing.

Initially one should check for correct line ID, but as said above, the automatic line IDs are typically incorrect, requiring the lines to be cleared and re-identified using the "i" key. Below are listed a sample line ID (taken from the example above).

Pixel	Wavelength	Line ID
47.78	74619.2101	74670
63.93	78813.4841	78750
88.50	85166.8354	85140
99.62	88033.285	88020
126.45	94941.4424	95030
156.33	102622.713	102600
213.27	117303.511	117280
257.31	128759.52	128770

In the figure and table below, we show a spectra taken in worse (wetter) conditions and with a wider slit. The line identification is less certain and fewer lines are indentified, leading to a worse confidence in the spectral fit.

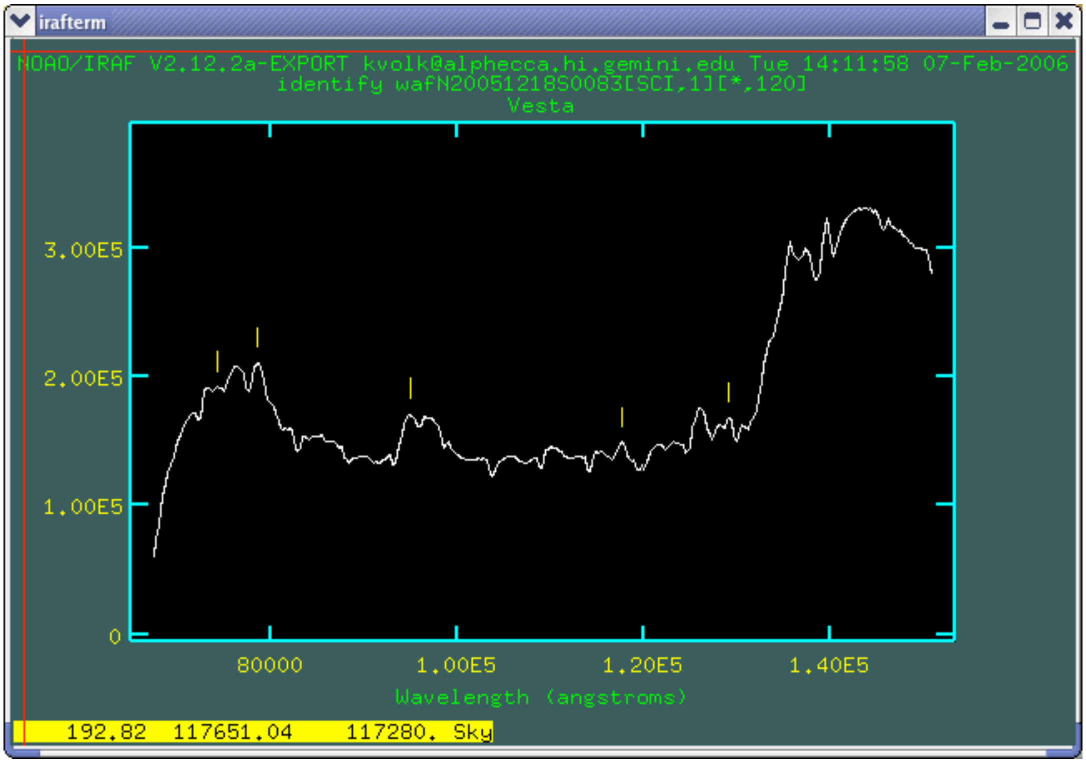

Figure 21. N band spectra during the line ID phase, using data taken in wet conditions with a wide slit.

Pixel	Wavelength	Line ID
26.88	74568.0089	74670
43.82	78907.1222	78750
106.18	94944.751	95030
192.82	117330.486	117280
237.00	128749.632	128770

Finally, below we show the line ID for a Q band spectra. In the Q band, the atmospheric bands are generally stronger than in the N band. In almost all cases, all 13 spectral features shown below are present.

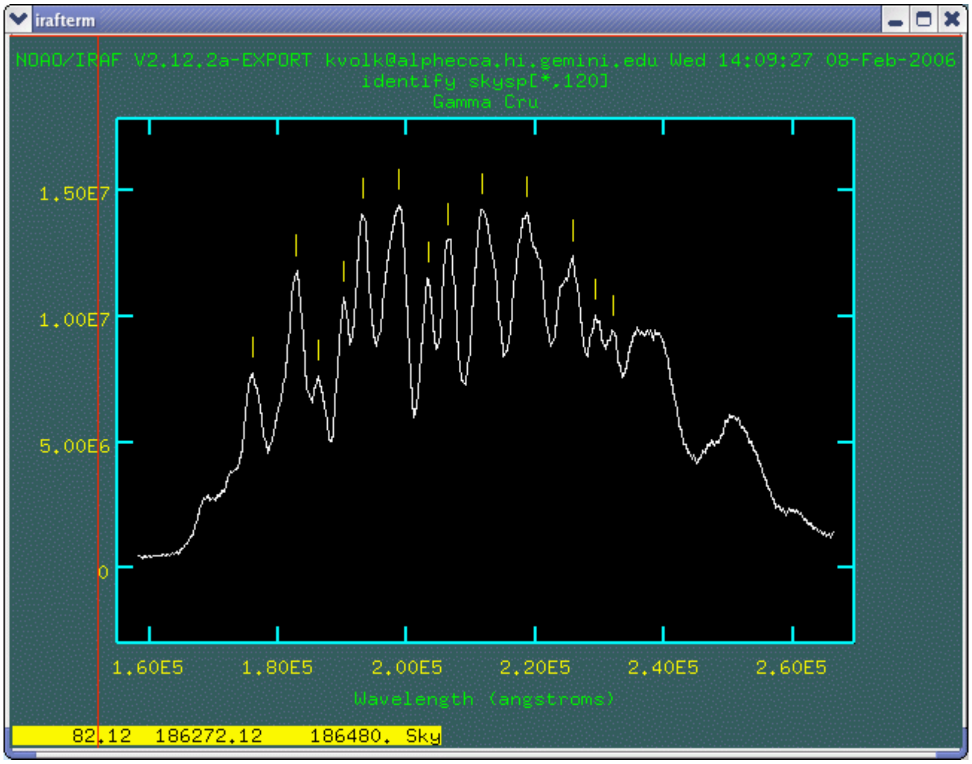

Figure 22. Q band spectra during the line ID phase, using data taken in typical conditions with a standard slit.

Pixel	Wavelength	Line ID
61.83	175780.171	175860
83.68	182971.936	182980
94.70	186596.989	186480
105.69	190216.019	190150
114.53	193123.953	193100
131.93	198851.61	198900
145.20	203220.359	203220
155.23	206521.998	206530
170.89	211676.384	211750
191.69	218524.299	218550
213.93	225844.891	225950
224.97	229478.821	229410
232.82	232062.571	231990

4.4.4 Wavelength Transformation

After the initial line identification, the IRAF tasks then seek to identify the same lines in the spectra in other parts of the sky spectrum, since the sky fills the slit/array completely. In most cases this can be achieved automatically, but there are rare cases when this automation fails and it is necessary to report this process interactively. Once the lines have been identified across the spectral image, a transformation is calculated from pixel position to wavelength, and this is applied to the spectrum when it is extracted in the next step.

4.4.5 Spectral Extraction

The spectrum can be extracted using the IRAF NOAO twodspec package, apall. To extract the spectrum a cut is made across the differenced spectrum and then this is traced across the dispersion direction. For brighter objects this is routine, but in fainter objects the apall command can fail due to lack of flux.

One should typically set the fl_extract of apall to "yes" so that the tracing can be interactively examined. Usually points the to far left and right of the spectra are unreliable, as typically the spectrum is spread out over only ~90% of the array, and hence the ends of the spectra are noise. In the case of CanariCam, the spectra are not curved and hence the tracing should be approximately flat (<1 pixel across the detector). Also, the spectral tracing should be close to linear. If either of these cases are not met from automatic tracing, points should be excluded until a reasonable tracing is obtained.

An example of a good tracing is shown below, and note that points were deleted to the left and right of the main spectra. Tracing of the spectra can be lost at shorter or longer wavelengths due to strong and variable water bands in these regions, so there is no absolute wavelength cut-on/off, rather it is condition dependant. In the case below, as the aperture used is 6 pixels wide, a linear fit would have provided just as good a fit than the curved fit shown.

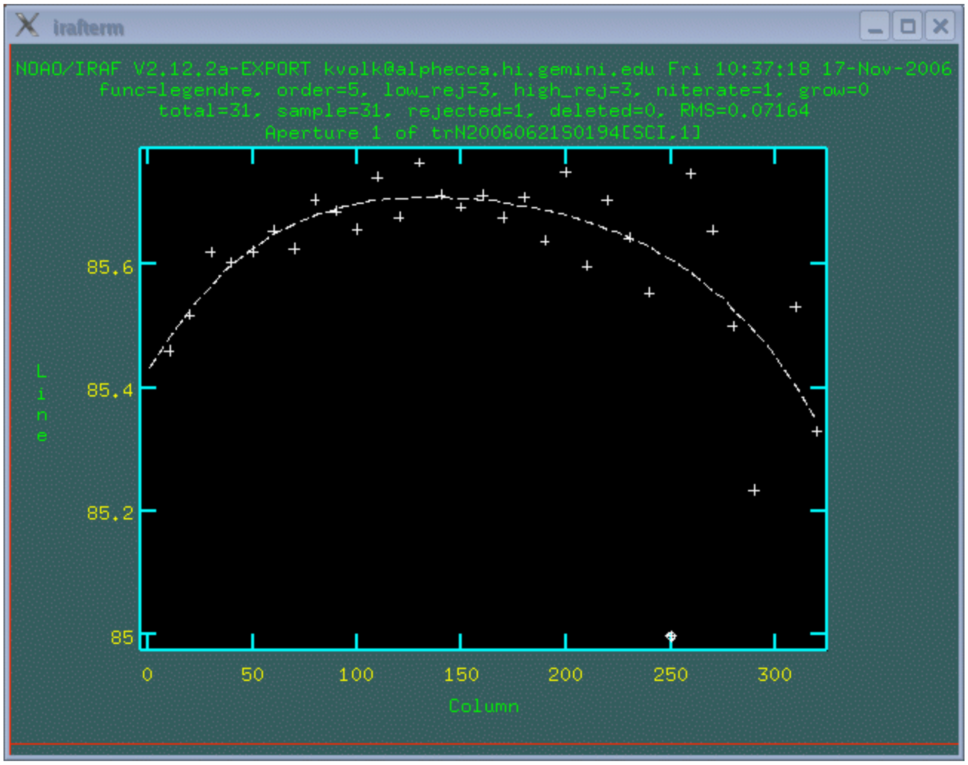

Figure 23. Spectral extraction curve.

4.4.6 De-fringing of Spectra

MIR spectra can be subject to fringing, especially at moderate spectral resolution; at low spectra resolution fringing is rarely observed. The fringes can be identified using fourier analysis and removed. This is an interactive step in the data reduction as finding the correct frequency to reduce in the fourier transformed spectrum cannot be achieved automatically. A strongly fringed spectrum taken with T-ReCS is shown below.

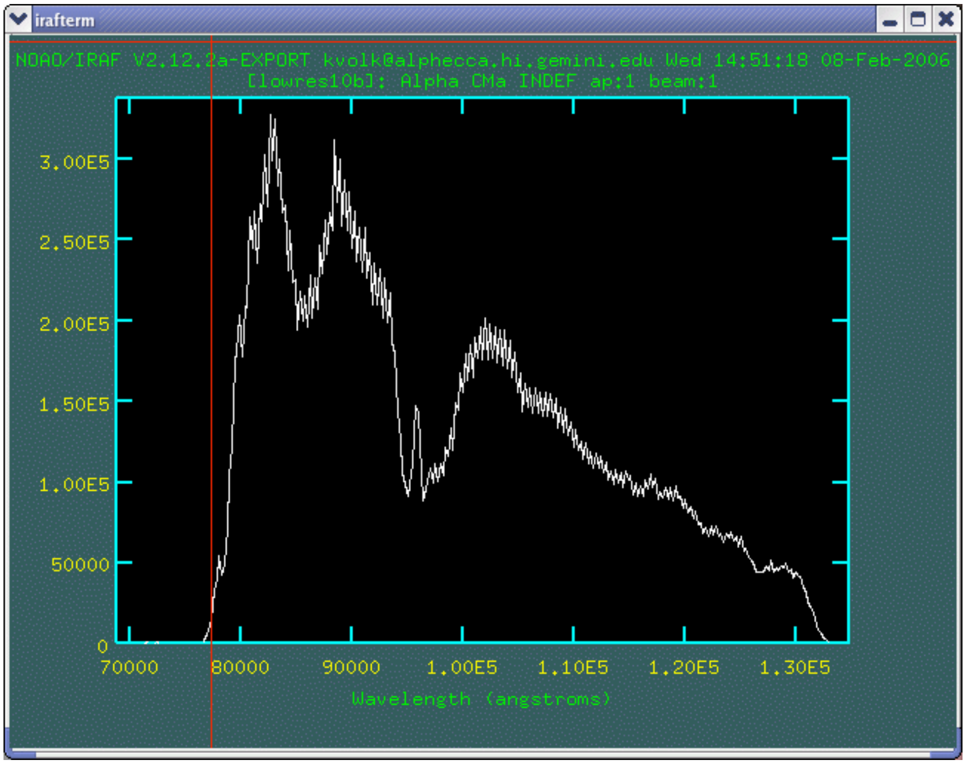

Figure 24. Fringed spectra.

The IRAF task msdefringe can be called to interactively fourier transform and remove the fringing from the spectra. When called, the task fourier transforms the spectra, and plots the real and imaginary spectra as a function of frequency. In the case of low-resolution fringing, only the highest frequency component is necessary to remove. One can set the range of components that are to be removed and replace these values by either zero or an interpolated value from the end points. A second option is to remove all negative values, but this often fails especially if the baseline level if slight offset to negative. Below is the fourier plot for the spectrum shown fringed above.

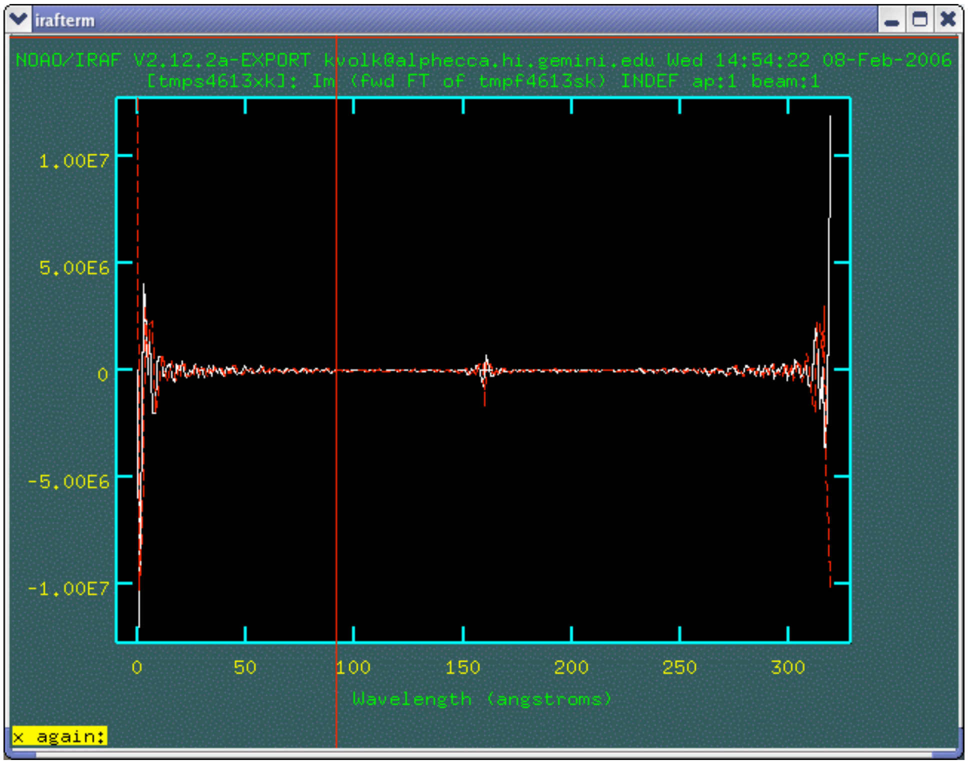

Figure 25. Fourier transform of a fringed spectra. The white curve is the real part, and the red curve is the imaginary part. One usually looks for the fringes in the real part.

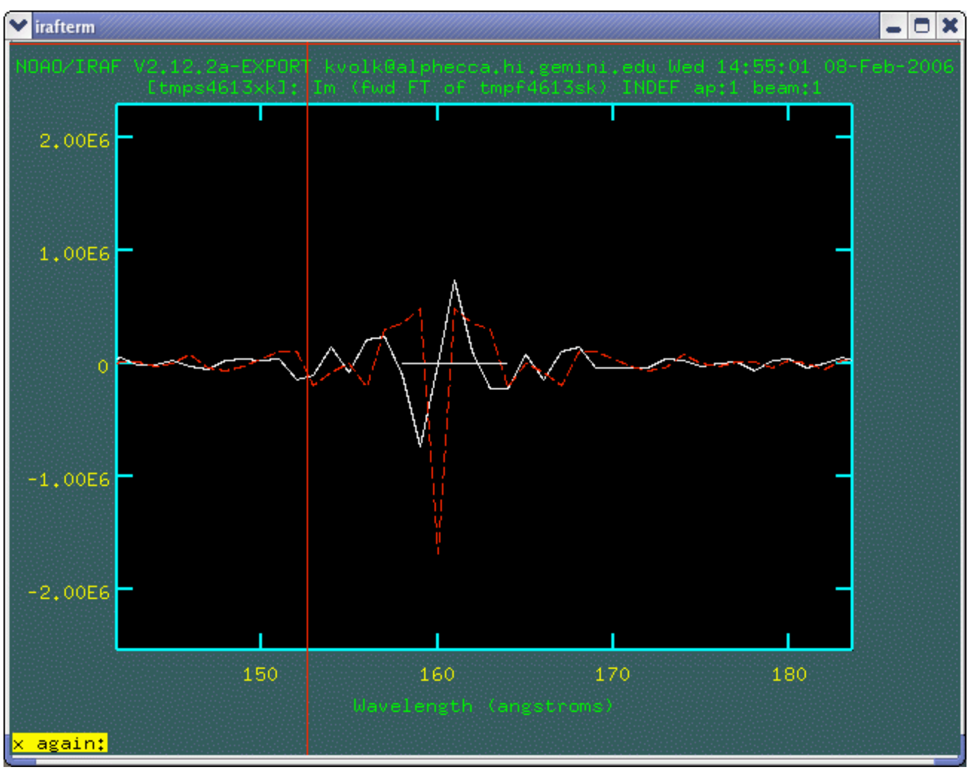

Figure 26. A zoomed-in image of the fourier spectrum, where the white horizontal line shows the filtered real and imaginary parts of the spectrum.

After exiting from the fourier domain plot (as usual in IRAF, using the "q" key), the image below is displayed, showing the original and de-fringed spectra. If the de-fringing was successful, the program is exited with the "r" key, or to exit and reject the de-fringed spectra this is achieved with the "i" key.

4.4.7 Spectral Flux Calibration

Spectral flux calibration is achieved with the msabsflux task. This in turn calls the telluric task in the IRAF NOAO onedspec package. In most cases it is wise to carry out this step interactively, since the automatically found "best" spectrum often is not actually what is wanted, especially for low resolution spectra, typically due to having large regions of little or no signal in the source and calibration spectra. Noise in these regions can often produce absurdly large signals in the resultant spectra, which severely skews the chi-squared minimization used in the IRAF telluric task to find the optimum shift between the two spectra.

In view of this problem the first thing one should do in running the task interactively is to window the plot to exclude the long and short wavelength regions with little or no signal. This is typically the wavelengths > 13 μm and < 7.5 μm.

One way to proceed is to set *:offset 0.* and *:dscale 0* so only one "output" spectrum is plotted in the upper panel. Scaling can usually be found that shows the proposed output spectrum fairly well. Then one needs to search the parameter space to get a good output spectrum. It is generally best to change the shift value with the *:shift* command. Shifts are usually small, so starting at zero and then checking values slightly positive and negative from there is usually helpful, where the main goal is to choose a shift that removes the ozone feature as well as possible. Wrong shifts cause the edges of the band to no longer match leaving a residual feature that tends to show up at around 9.3 - 9.6 μm

The following figures show:

1. The initial plot screen
2. The plot screen once the wavelength range has been restricted
3. The plot screen when the shift has been set to 0 pixels

In the final case, no shift produces a nice, smooth output spectrum over the region seen in the plot. And the final result is the spectrum of an asteroid so what is seen is something that is very close to a 217 K blackbody shape

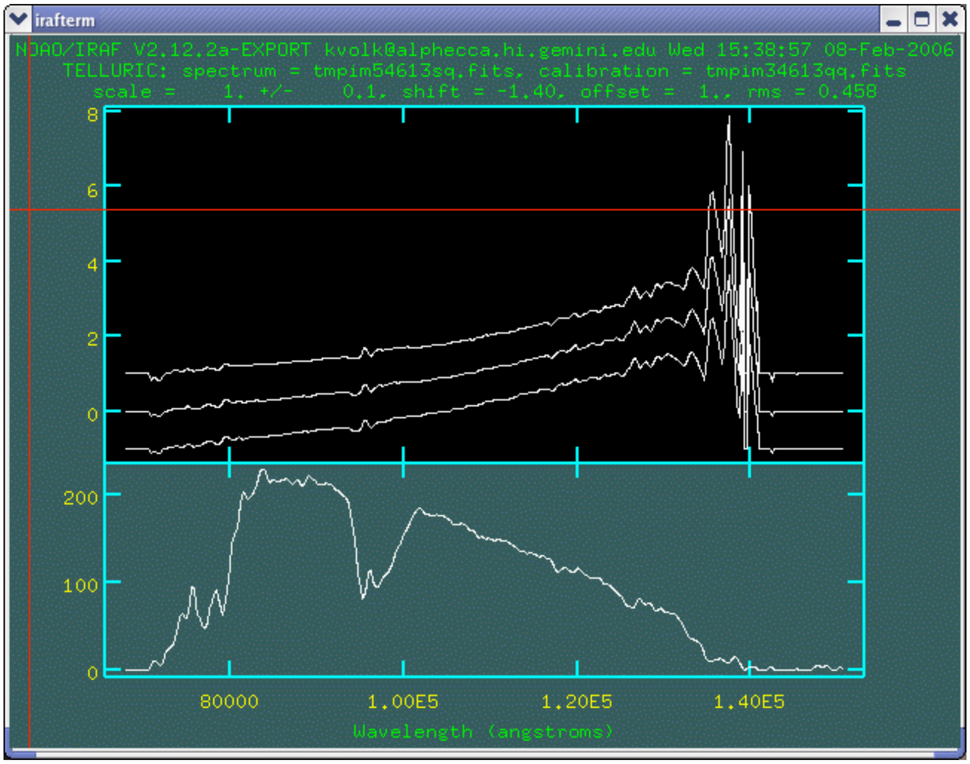

Figure 27. The initial plot with a -1.4 pixel shift as found by the telluric task.

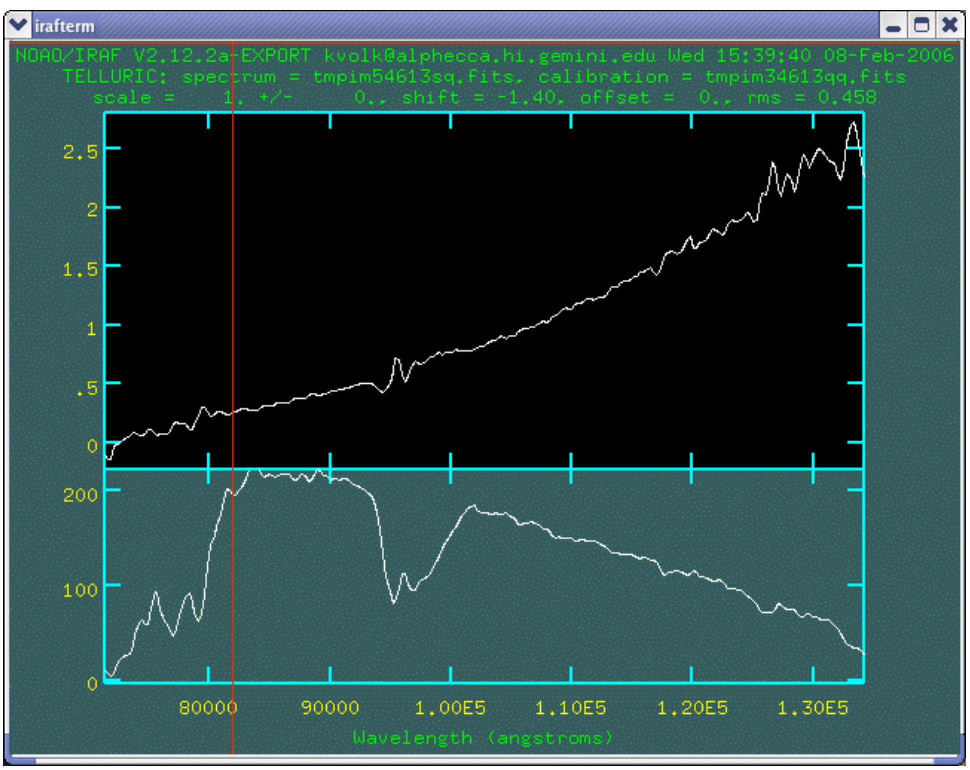

Figure 28. The plot after changing the range and setting the offset, as well as setting dscale to 0.0.

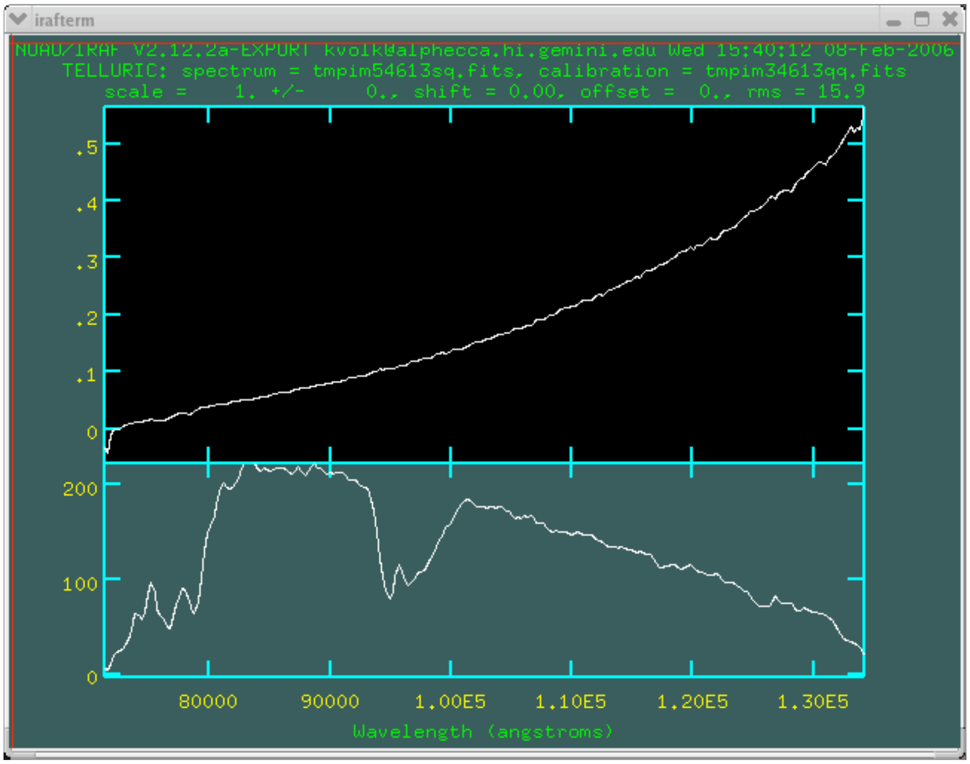

Figure 29. The plot with a shift of 0.0 pixels.

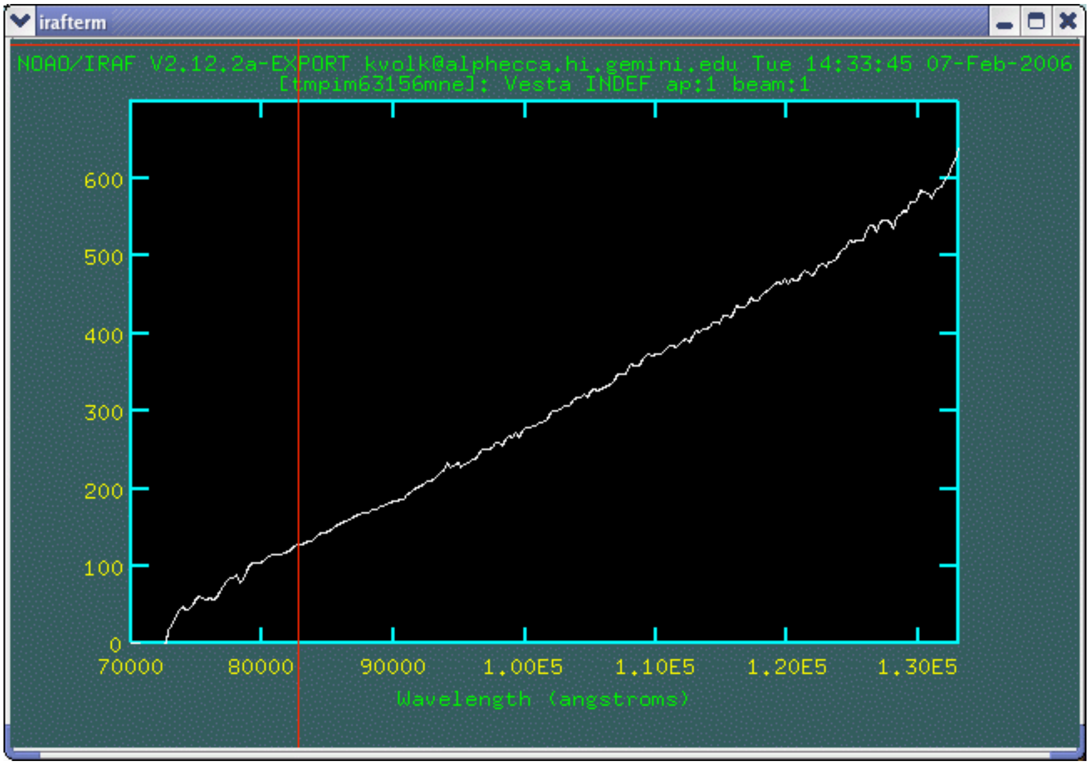

Figure 30. The final, flux and wavelength calibrated spectrum of the asteroid Vesta.

4.5 CanariCam Polarimetry Data Reduction

The process of polarimetry data reduction is initially very similar to that of imaging data reduction, but where the position angle (PA) of the half wave plate (HWP) is used to separate (i.e. no combine) the files. The exact methodology of data collection for CanariCam polarimetry is to be defined during commissioning of CanariCam (as the sky, telescope and instrument will have a fundamental effect on the data collection) and hence this data reduction after the following steps have been taken:

1. The chop-nod correction has been completed
2. Files are stored and accessible in any naming convention, but that the fitsheaders are maintained as written by CanariCam
3. The files to be operated on have similar sky background, image quality and noise features

When using CanariCam in polarimetric mode, we use the instrument in effectively imaging or spectroscopy, but with the additional following components (in order) in the beam:

1. Focal plane mask
2. Half wave plate
3. Wollaston prism

The HWP is used to modulate (rotate the PA of polarization) observed by the Wollastron prism rather than rotating the instrument. A mechanical rotation of θ results in an optical rotation of 2θ, and as one typically wants to sample the polarization at any PA, the HWP must be (mechanically) rotated to a minimum of 0° and 22.5°, but as a confirmation, the angles of 45° and 67.5° are typically used (for more on polarimetry basics, the reader is referred to the polpack manual (http://star-www.rl.ac.uk/star/dvi/sun223.htx/sun223.html) or any of the many discussions of polarimetry data collection in the literature. The Wollaston prism is the analyzer which splits the incident beam into two beams that are perpendicularly polarized. The beam that passes through the prism that is undeviated is called the "ordinary" beam (or o ray), whereas the deviated beam is called the extraordinary beam (or e ray). Both beams are recorded simultaneously on the array, and hence for each object (or patch of sky) in the field of view, two perpendicularly polarized images are formed on the array. For this reason, it is typical to use the polarimetric mask in the aperture wheel to obscure 50% of the field of view. This prevents overlapping of the images or crosstalk from residual sky emission.

As CanariCam uses two transmissive components (the HWP and Wollaston prism), there are two key chromatic effects. The separation of the o and e beams is a function of wavelength, as shown in figure 31 below from lab measurements. This change in dispersion versus wavelength is an interesting effect for imaging, and one should note the change when performing the polarimetric data reduction. In spectropolarimetry mode, the resultant spectra will be curved, and again this must be noted when extracting the spectrum.

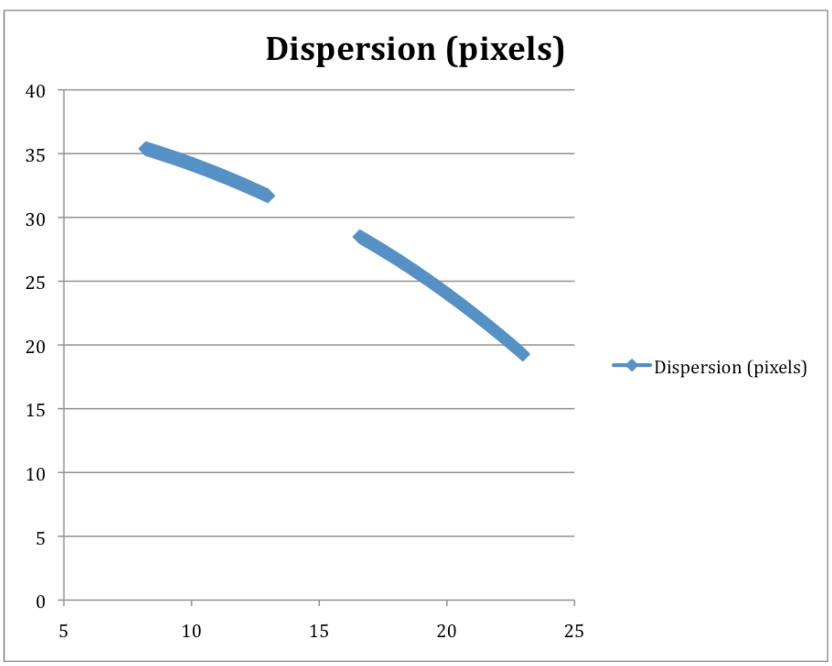

Figure 31. Measured polarimetric dispersion (measured in pixels) versus wavelength (μm) for the CanariCam Wollaston prism.

In addition to the varying separation between the o and e-rays, the chromatic effect means that in broadband filters (such as the N band filter), there is a slight elongation of the derived PSF along the polarimetric dispersion direction. It is expected that image quality degradation due to atmospheric conditions, guiding errors or other issues will dominate over this elongation, but one should still be aware of this issues, as shown in figure 32 below. In this example, a monochromatic source at 10.5µm (Strehl ratio 98%) is compared to a polychromatic source at 7.5, 10.5 and 13.5µm (Strehl ratio 81%), and hence is very much a worst-case scenario, very unlikely to be replicated in observational conditions.

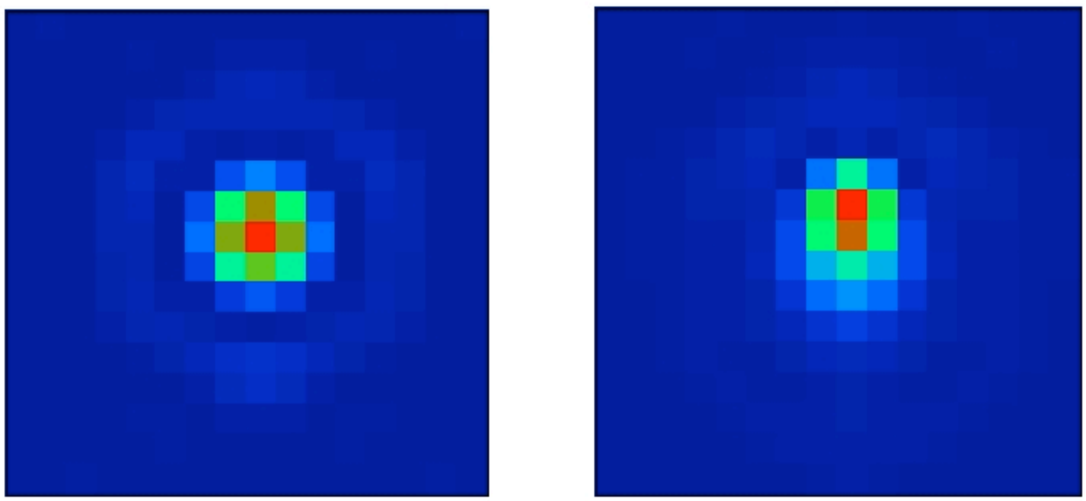

Figure 32 Monochromatic 10.5µm o-ray image (left) and polychromatic o ray image (right).

A further complication in polarimetry mode arises as the HWP retards the beam by half a wave at one wavelength only (10.0µm). That is, the retardation is a function of wavelength, with the optimal (efficiency of retardation = 100%) occurring at a single wavelength. The roll-off in retardance and efficiency (as a function of wavelength) is shown below in Figure 33. This response was measured in the laboratory, and will be re-determined during CanariCam commissioning on-sky. The result is that for a 100% polarized source measured at 10µm, CanariCam measures 100% polarization, whereas for a 100% polarized source measured at 8µm, CanariCam measures 80% polarization. One must note these values are for monochromatic light, and so for both broad and narrow band filters centered even close to 10µm, a polarimetric efficiency correction must be made. As the response is of the HWP efficiency vs. wavelength has been well characterized in the lab, a simple multiplicative correction is required to report the true degree of polarization – the position angle (PA) of polarization in unaltered by the HWP efficiency.

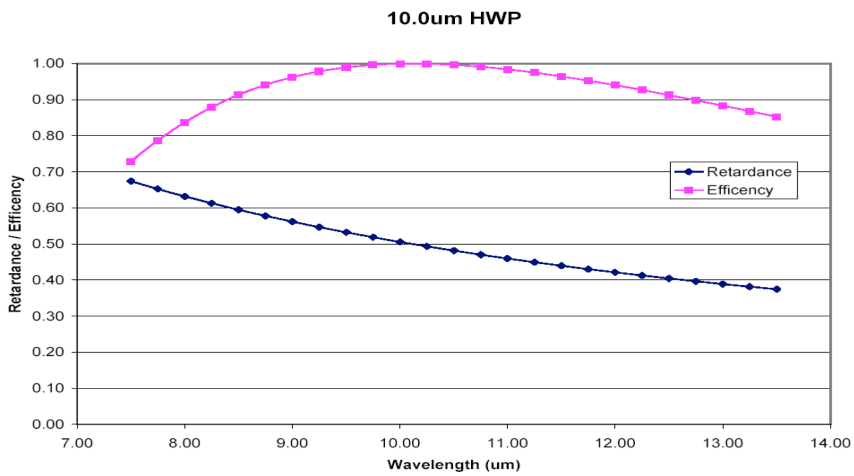

Figure 33 Retardance and efficiency of the CanariCam 10µm HWP as a function of wavelength.

The essential data reduction for the data is described in the following section. Data is collected using the standard chop-nod procedure of MIR observations, but we note that currently it is unclear how many HWP PAs will be required to give an optimal polarimetric signal per nod position. This is an essential task for commissioning of the CanariCam polarimetric mode. It is crucial to note that the images are not stacked across HWP PAs, if this is done, the polarimetric data is lost. Rather, one should ensure the data is processed with particular attention paid to the HWP PA.

4.5.1 Data Reduction Overview

The essential data reduction steps for CanariCam polarimetry are:

1. Perform the chop-nod correction, as for standard imaging data reduction
2. Extract the o and e rays, nothing the HWP PA used
3. Align the images. This is a crucial step, as a misalignment, especially where there is a strong flux gradient, can lead to very high spurious polarizations at highly variable PA.
4. The polarization is calculated by estimating the Stokes parameters for each resolution element. The Stokes parameters used in linear polarimetry are I (total intensity), Q (horizontally polarized) and U (vertically polarized).
    a. The Stokes parameters are typically estimated using standard algorithms, as discussed here (http://www.starlink.rl.ac.uk/star/docs/sun223.htx/sun223.html and http://www.starlink.rl.ac.uk/star/docs/sun223.htx/node61.html#APP:POL).
5. Once the Stokes parameters have been estimated, the degree of polarization can be estimated using the relationships (also described here http://www.starlink.rl.ac.uk/star/docs/sun223.htx/node15.html):

$$
\begin{aligned}
I_p &= \sqrt{Q^2 + U^2} \\
p &= I_p / I
\end{aligned}
$$

$$\theta = 0.5.\arctan(U/Q)$$

6. Polarimetric data is perhaps best displayed as a series of polarization vectors overlaid on a total intensity image of the source. The length of the polarization vector is proportional to the degree of polarization and the PA of the vector is representative of the PA of polarization. Software tools exist to take the I, Q and U Stokes images and produce those vectors.
7. Finally, measurements of the images and vectors can be performed using standard image display tools.

There are few polarimetry data reduction tools generally available to the astronomical community, with the notable exception of the Starlink program polpack. This program is the most widely available and also most user friendly program the authors are aware of, and hence we recommend use of this program to reduce CanariCam polarimetry data. To run this program, the Starlink software suite should be installed, available free of charge from http://starlink.jach.hawaii.edu/starlink. We suggest the whole standard package is installed, which will include the following key packages:

- Polpack
- Gaia
- Convert

4.5.2 Data Reduction Steps

The data should be reduced using IRAF to the stage where there are multiple chop-nod corrected files, taken at a variety of HWP PAs. Do not stack the images. Should one wish to check the HWP PA, this is recorded in the fitsheader. The software that will automatically make the chop-nod correction, outputting a series of un-stacked files at their respective HWP PAs will be produced after commissioning, but this task can be trivially performed using the wfits IRAF command. The result will be several files (a multiple of 4, as there are 4 HWP PAs) in the directory. Starlink operates not on .fits files, but .sdf (exactly equivalent to .ndf), and hence one must convert the CanariCam .fits files to CanariCam .sdf files. To do this, once must start the conversion program and convert all files (*) by typing:

1. convert
2. fits2ndf *

A set of .sdf files are now in the same directory as the .fits files. Next the polpack GUI (graphical user interface) should be started, with the commands

1. polpack
2. polka *

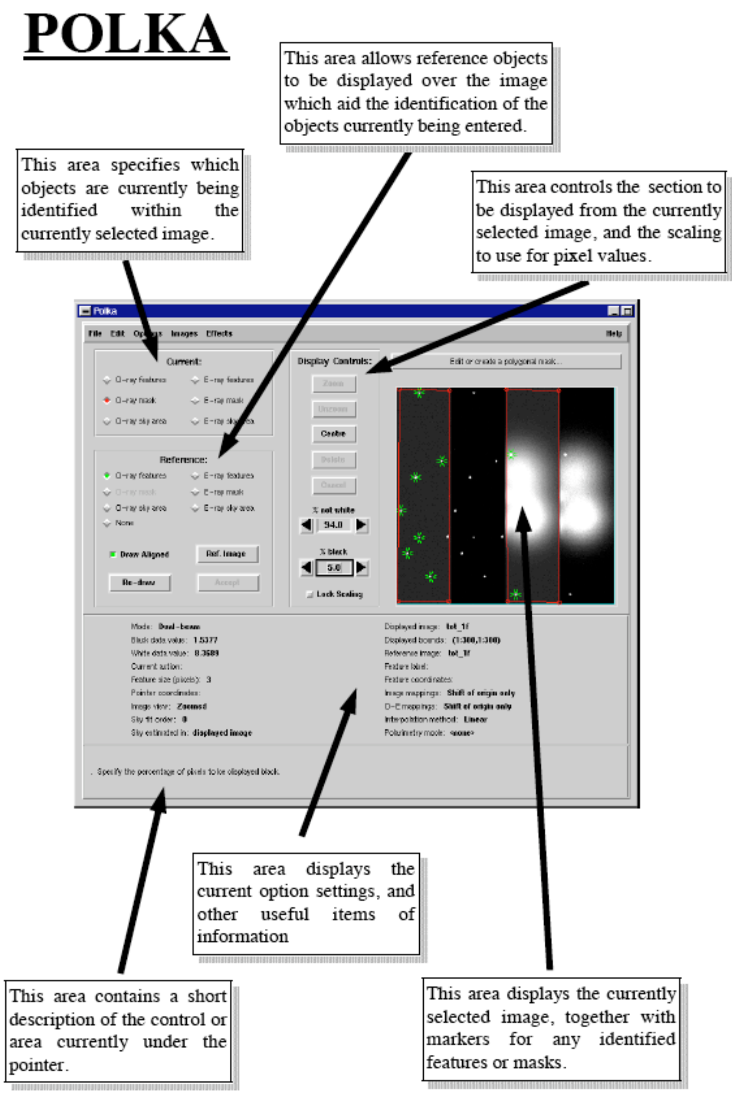

Figure 34 The POLKA graphical user interface.

The polka GUI is the crucial part of the CanariCam polarimetry data reduction. Polka 'knows' the HWP PA as it interrogates the fitsheader, and with a few more inputs through the GUI, the polarimetry can be trivially reduced. The polka GUI is split into three areas, the dialogue boxes, the graysacle image of the polarimetric image and the status panel. The suggested inputs are:

a. In the options menu, turn off sky subtraction (this has already been performed in the MIR data reduction steps before. Also in the options tab, dual beam mode should be selected.
b. Next an o-ray feature should be defined. Ideally this is an object that can be easily centroided in any of the polarimetric slots. If necessary, some of the images may need to be co-added to increase the source's S/N, in which case one should quit polka and perform this step and re-start polka. The o-ray feature should be first selected on the current panel of the dialogue window, and then a feature selected on the image.

c. Next the user should select the e-ray feature on the dialogue window and a the same feature selected in the e-ray image.
d. This process can be repeated for more than one source, should this be available.
e. Next the o-ray area to be extracted should be selected. Click first on the o-ray mask in the dialogue box, and then click on the image to define the polynomial extraction area.
f. The e-ray area to be extracted is automatically calculated from knowledge found in sections b, c and d, and can be shown by clicking on the e-ray mask in reference.
g. This information can be transferred to all images by using the image menu, selecting all and then clicking on the transfer button.
h. The I, Q and U images are calculated when one clicks on the file menu and selects exit. This process is automatic, very reliable but can take some time.
i. The final image output has three planes, and they are the I, Q and U images.

The vector map maybe produced through use of the polvec command of polpack, which converts the I, Q, and U images to a vector map. Should one want to bin the polarization vectors to achieve a higher S/N, this can be accomplished using the polbin command of polpack.

To display the eventual image, the optimal image display tool is gaia. In gaia, the polarization vectors can be over-plotted on the total flux image by selecting the polarimetry toolbox in gaia and selecting the appropriate vector catalogue. One can measure the degree of polarization, PA, polarized flux and several other parameters using this tool.

Much more details about polpack are found in the manual and the interested user is strongly recommended to read that document for more details.

4.5 CanariCam Coronography Data Reduction

The coronographic mode of CanariCam, with respects to data reduction, is a subset of imaging, and hence all data reduction mechanisms envisioned for this mode are exactly the same as discussed in imaging above.

Appendix A : Mid-IR Astronomy

.

I The Atmosphere

The Earth's atmosphere is not completely transparent to mid-IR radiation. As shown in Figure 35, the atmospheric transmission through the mid-IR regime has numerous strong absorption features caused by the Earth's atmosphere. Ozone (O_3) is responsible for many of these features including the strong absorption at 9.6 μm, while CO_2 causes the mid-IR transmission to drop to zero between 14 – 16 μm. Water vapor also absorbs in the mid-IR and results in many of the absorption features such as those seen in the wavelength regime between 16 – 30 μm. At $\lambda > 40$ μm, the atmosphere is primarily opaque to radiation until the submillimeter regime. Astronomers typically observe at wavelengths where the atmospheric transmission is the highest, refereed to as atmospheric "windows". In the mid-IR there are two major windows. The first is located between 8 - 14 μm while the second is located between 16 – 30 μm, often called the 10 and 20 μm windows respectively. Within these mid-infrared windows, there can be rapid variations in transmission due to changes in the water vapor column depth. This can be seen in the change of transmission in Figure 35 when the atmospheric water vapor changes from 1.0 mm to 3.0 mm. In addition to absorption, the atmosphere also emits strongly in the mid-IR peaking at ~ 10μm. Thus the atmosphere not only attenuates the mid-IR signal from an astronomical source, but also dilutes the signal with thermal emission of its own. Separating the background sky emission from the source emission is one of the key elements in observational mid-IR astronomy.

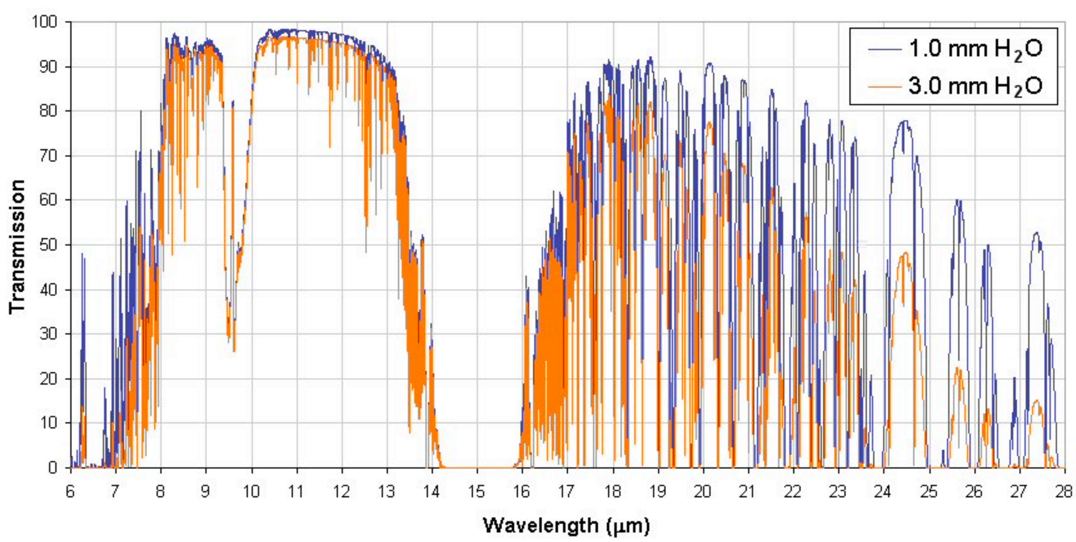

Figure 35. Atmospheric transmission at Mauna Kea, Hawaii. The 7-14 micron window can be seen clearly. Longer wavelength filters take advantage of the 16-30 micron window, which has numerous absorption features. (Image adapted from ATRAN model (Lord, S.D. 1992) and data from Gemini Observatory)

Another affect the atmosphere has on observations is “seeing”. This is a blurring affect caused by turbulence (density inhomogeneities in the atmosphere). This results in random fluctuations in refraction causing a star to vary in intensity and location on the sky (scintillate). This effect limits the angular resolution of all but the smallest optical telescopes. Ideally the image of a point-like source in the focal plane of a telescope should resemble a classical Airy disk. In practice however, time-averaged images resemble a two dimensional Gaussian distribution with a full width at half max rarely smaller than 1” at optical wavelengths. Seeing however is wavelength dependent with image size proportional to ~ $\lambda^{-0.2}$. Therefore longer wavelength mid-IR observations are much less affected by this phenomenon. This results in mid-IR images being primarily diffraction limited.

II Background Subtraction

The primary characteristic of ground-based mid-infrared (5−30 μm) astronomy is high background photon flux. The source of this background flux is the combined emission from the atmosphere, the telescope mirrors, and the entrance window of the cryostat that houses the camera optics and detector. For example, using T-ReCS on GTC South with the PAH2 filter ((λo = 8.6 μm, $\Delta\lambda$ = 0.437 μm) we observe a photon flux on the detector equal to ~ 1.13×10^9 photons pixel^{-1} s^{-1}. This will fill the wells to ~ 60 % in 50 ms assuming a quantum yield ηG of 0.40 and a well depth of 3.0×10^7 electrons (low gain mode). If the data from each pixel of the 320 × 240 array are digitized at 16 bits (i.e. 2 bytes), the corresponding data rate is ~ 3.0 Mbytes/s. The short frame integration time therefore requires fast electronics to handle these high data rates.

From an astronomical perspective, these high background fluxes have a more serious consequence than just the necessity of fast acquisition electronics—astronomical objects of interest are invariably ***much fainter*** than the background emission. Thus, very precise subtraction of this background flux is required to extract the signal of interest. For example, typical bright infrared standard stars used for flux calibration are frequently an order of magnitude fainter than the background emission. And, scientifically interesting astronomical objects may be fainter than the background emission by ***four or more*** orders of magnitude.

II.I The Standard Chop-Nod Technique

The requirement of precise background subtraction dictates the method by which images are acquired at a telescope. Background subtraction is effected in real time using the standard infrared astronomical “chop/nod” technique. In this technique, the telescope is pointed at an object of interest (the “program object”) and the camera acquires a set of images. An image consists of signal from the program object added onto the much larger signal from the background. The secondary mirror of the telescope is then moved slightly away from the nominal position so that the program object moves out of the field of view of the camera and another set of images is acquired. This procedure, called a “chop” cycle, is repeated many times at typically a 2-10 Hz rate moving back and forth between "on-source" and "off-source" positions. A "chop-differenced" signal is formed by taking the difference between the on-source and off-source images.

While this rapid movement of the secondary mirror allows subtraction of a spatially uniform background that is varying in time at frequencies below the chop frequency, it usually still contains a spurious signal that may still be significantly larger than the source signal. This signal, termed the "radiative offset," results from the fact that the emission pattern of the telescope, as seen by the camera, depends on the optical configuration of the telescope. Movement of the secondary mirror changes this configuration, resulting in two different emission patterns. The difference in these emission patterns is found in the chop-differenced signal.

In order to remove the radiative offset, the entire telescope is moved after a short period of time so that the source now appears in what was previously the off-source position of the secondary mirror. This movement of the telescope is termed a "beam switch" or "nod" and typically occurs on timescales of tens of seconds. Timescales are much longer than that used in chopping due to slower changes in telescope emission relative to sky emission. Chop-differenced frames are then formed with this new on-source and off-source configuration. In this new configuration, the radiative offset will have changed sign and is effectively canceled when the new chop-differenced data is added to the old chop-differenced data (provided the telescope emission has not changed in the time between beam switching).

Figure 36 demonstrates the acquisition of data in the standard "chop/nod" mode. The images shown here were obtained with University of Florida mid-infrared imager/spectrometer OSCIR at the NASA Infrared Telescope Facility in Hawaii (IRTF). The top row of four images shows the raw data frames from the two secondary mirror positions at each of the two nod positions (called "Nod Position A" and "Nod Position B") of the telescope. These images are dominated by fixed-pattern offsets due to pixel-to-pixel variations and offsets between the 16 channels of the acquisition electronics. The background counts in these raw images correspond to 7.4×10^{8} electrons s^{-1}. Each raw image consists of 5 minutes of total integration time (i.e. 15,000 frames coadded using a 20 ms frame integration time and the N-band filter) obtained in the chop/nod sequence as described above. The second row of two images shows the "chop-differenced" data derived from the subtraction of the on-source and off-source data in the two nod positions of the telescope. Note that the dominant pattern (principally a gradient along the diagonal connecting the lower-left to upper-right corners of the images) changes sign between the two chop-differenced frames. However, since the subtraction is always done as "on-source minus off-source", the source signal remains positive in both chop-differenced frames. The signal levels in these differenced frames range $\pm\ 3.2\times10^{6}$ electrons s^{-1}, which is ~ 0.4% of the raw background signal. Finally, the bottom row shows the net signal obtained by adding together the two chop-differenced frames shown in the middle row (note that no other processing has been done to the data other than the additions and subtractions as described above). The detected source is the nuclear region of the starburst galaxy NGC 253. The net signal is the result of a total exposure of ~ 20 minutes in which half that time is actually spent imaging the off-source "reference" position. The signal level at the "tail" of this source near the middle of the frame is ~ 6.4×10^4 electrons s^{-1}. This is about four orders of magnitude below the background level shown in the raw frame. In fact, the signal-to-noise ratio at this level in each pixel is about seven, so that the effective background subtraction is more nearly five orders of magnitude below the background!

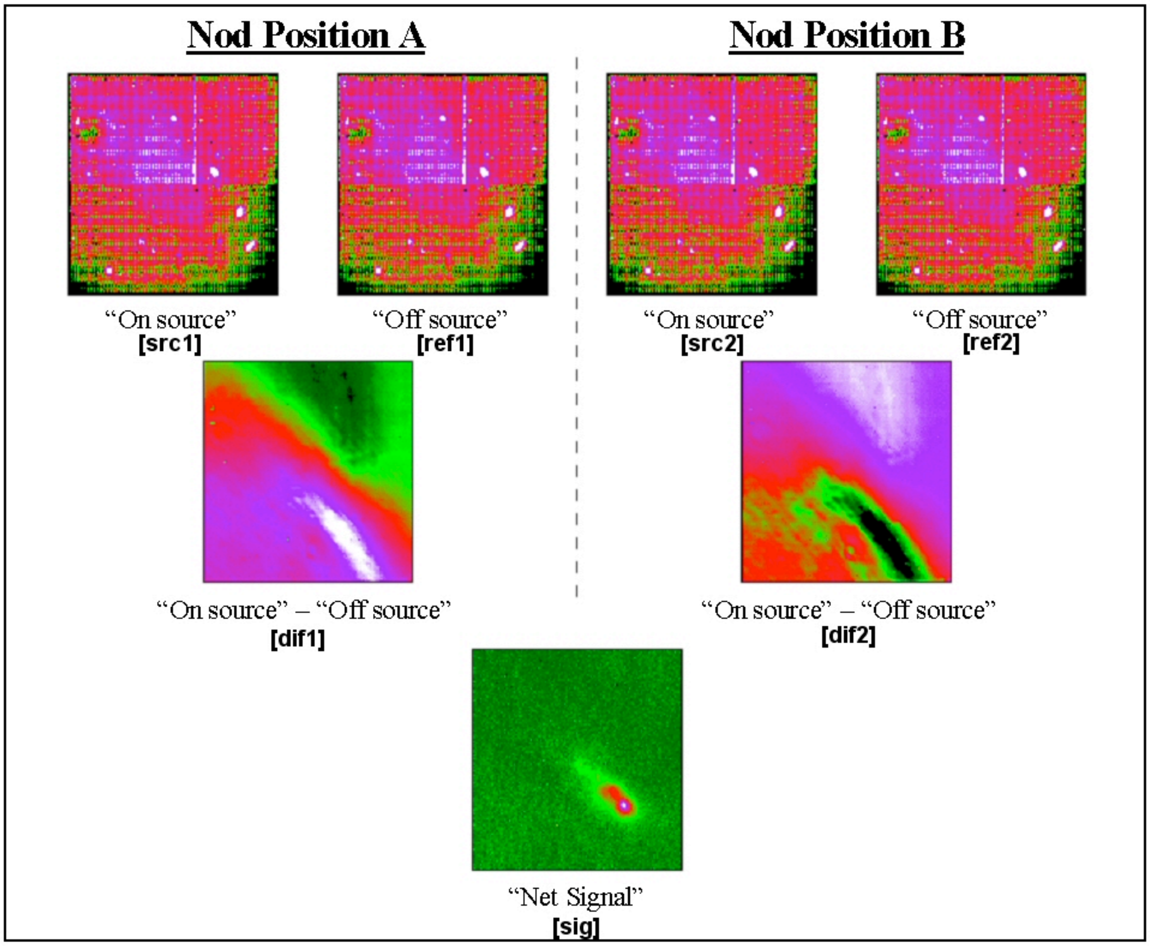

Figure 36. Illustration of standard chop-nod technique. Common terminology or short hand for the individual frames is given in brackets [] (see Table 12)

While a typical frame time is 20 ms, the CanariCam electronics can handle frame times as short as 2.5 ms. However, data are not saved at this rate. Rather, the electronics is designed to coadd data from the two positions of the secondary mirror into two separate "chop" buffers. For astronomical observations data will be typically saved at a rate of one pair every two seconds.

Table 12 Common Chop-Nod Terminology

Term	Description
src1	refers to “on-source” image in Nod position A
ref1	refers to “off-source” image in Nod position A
dif1	refers to src1-ref1 (difference of on and off source for Nod A)
src2	refers to “on-source” image in Nod position B
ref2	refers to “off-source” image in Nod position B
dif2	refers to src2-ref2 (difference of on and off source for Nod B)
sig	refers to dif1+dif2 (net signal of observation from one chop-nod sequence)
sig_accum	refers to accumulation of sig frames throughout observation. After each chop-nod sequence a new sig is added to the sig_accum. (*this is used as the primary display during observations as it shows the final result of the chop-nod method)

II.II On-Chip Chop & Nod Method

Another standard method exists for executing chop/nod background subtraction. This method is referred to as the “on-chip” method and is demonstrated in Figure 37 with data obtained using OSCIR on the Keck-II Telescope in May 1998. In the on-chip method, the chopper throw is set to be less than the detector array field-of-view so that the source remains “on chip” in both chopper positions, i.e. in both the “on-source” and “off-source” chopper positions as referred to in the standard method. This on-chip chop can be seen by examining the top row of Figure 37 where, in this case, the source is bright enough to be seen in the raw frames. Note that since the source is present in both positions of the chopper, the chop-differenced frame will contain both a positive and negative image of the source as seen in the second row of Figure 37. The telescope beam switch is then made perpendicular to the chop throw (recall in the standard technique, the beam switch is parallel to the chop throw). The throw for the telescope beam switch is also set to be less than the array field-of-view so that the source remains on-chip. Again, a chop-differenced image is formed, resulting in both a positive and negative image of the source.

Whereas in the standard technique the beam switching resulting in a change of sign of the telescope radiative offset, in this technique the radiative offset has the same sign in both chop-differenced images. The radiative offset is removed and the net signal formed by taking the difference, rather than the sum, of the chop-differenced images. In this method, the net signal contains four images of the source in a box pattern, with the sources located at the vertices as demonstrated by the single image in the third row of Figure 37. Two of the source images are positive, and two are negative, with the pattern such that the positive source are diagonally opposed and the negative sources are diagonally opposed. In post processing, the final image is constructed by bisecting the net signal image into four pieces and then registering and stacking (with the appropriate sign change) to form the final image.

It is clear that the basic requirement to use this on-chip method is that the program source be spatially compact, i.e. less than ¼ of the array field-of-view. What is not so obvious is that while ***all*** of the source photons are collected with this technique, as opposed to only ***half*** of the source photons collected in the standard method, the source signal-to-noise ratio in the final image ends up being the ***same*** for both methods. This is a consequence of operating in the background limited noise regime and is discussed further in the next section.

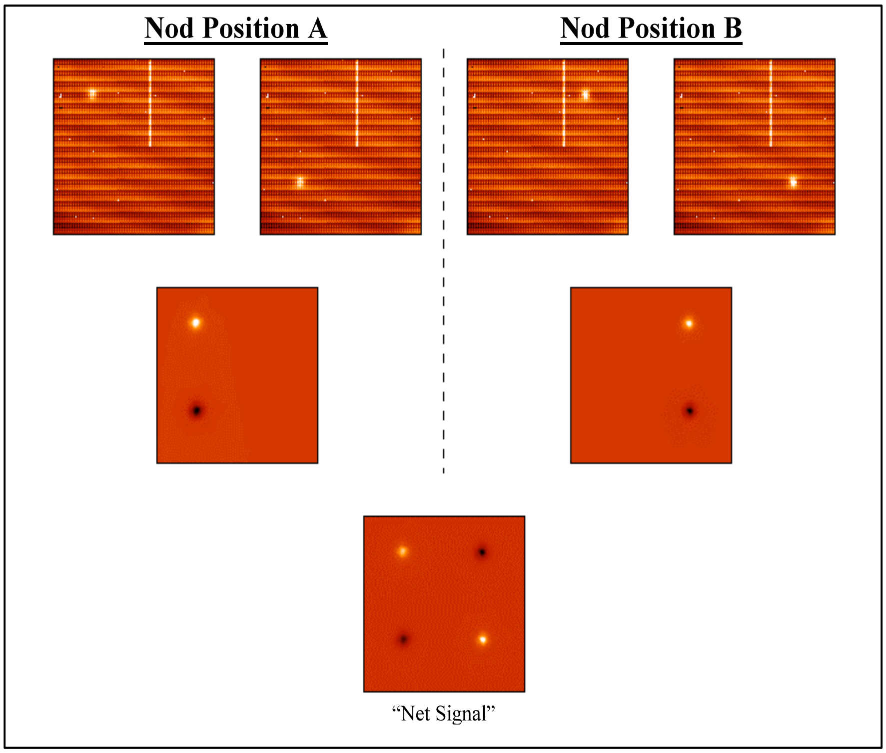

Figure 37. Illustration of the on-chip method.

II.III Comparison of Signal-to-Noise for Methods

In the "standard" chop-nod method described in Section II.I, only half of the total time spent accumulating photons is actually spent collecting source photons. On the other hand, in the "on-chip" method described in Section II.II, source photons are accumulated for the entire duration of the observation. It would therefore seem that, for a spatially compact source in which either method could be employed, the on-chip method would result in a larger source signal-to-noise ratio (S/N) than the standard method given the same total observation time. However, due to the fact that the observations are background noise limited, the ***signal-to-noise ratios are identical for a given observation time.***

For clarity, consider a chop-nod observation that consists of a single chop cycle and a single nod cycle. Therefore, the observations consist of the accumulation of *exactly* 4 frames of data. Let the "noise" in each of the 4 frames be given by σ_{frame}. Let the source signal in a single frame be given by S. In the standard chop-nod technique, each of the chop-differenced frames consists of the difference between one frame with the source and one frame without. Since the noise in resultant chop-differenced frames adds in quadrature, the S/N on the (*single*) source appearing in a chop-differenced frame is given by $S/(\sqrt{2}\cdot\sigma_{frame})$. The net signal is then formed by adding the two chop-differenced frames together. Noting that in the standard method the source images are located in exactly the same place in each of the two chop-differenced frames, the source signal doubles and the noise increases by $\sqrt{2}$ when the images are combined, so that the final S/N becomes S/σ_{frame}.

Next consider the on-chip technique. In this method, *each* of the 4 frames contains an image of the source with signal S and noise σ_{frame}. As described earlier in Section II.II, and as shown in Figure 37 the two chop-differenced frames will each contain two images of the source, one positive and one negative. The individual S/N of each of these source images is $S/(\sqrt{2}\cdot\sigma_{frame})$. This is, of course, the same as for the single source image in each of the two chop-differenced frames as derived for the standard method. Now, the net signal is formed by taking the difference of the two chop-differenced frames. The net signal frame contains four images of the source, two positive and two negative. The key point here is that in forming this net signal difference the positive and negative images in a given chop-differenced frame are each combined with a portion of the other chop-differenced frame which *does not contain signal*—recall in the standard method that the single source image in each chop-differenced frame is located at the *same* position. Therefore the S/N of each of the four source images in the net signal frame is *reduced* by $\sqrt{2}$ with respect to its value in the chop-differenced frames. This yields a S/N of $S/(2\cdot\sigma_{frame})$ per source image. The final image is formed by cutting the net signal frame into four pieces, each containing a single source image, registering them, and summing them. In this process, the source signal increases by a factor of 4, and the noise, taken in quadrature, increases by (i.e. $\sqrt{4}$). The final source S/N becomes $(4\cdot S)/(2\cdot 2\cdot\sigma_{frame})$ or S/σ_{frame}. This is the same S/N as obtained with the standard method. *Note well* that this only holds for the background photon limited noise regime.

.